IEEE Access
Multidisciplinary ⋮ Rapid Review ⋮ Open Access Journal

Received October 27, 2021, accepted November 18, 2021, date of publication November 23, 2021,
date of current version December 3, 2021.

Digital Object Identifier 10.1109/ACCESS.2021.3130296

Design of a Fixed-Wing UAV Controller Based on Adaptive Backstepping Sliding Mode Control Method

CHANGCHUN BAO[1], YUFEI GUO[2], LERU LUO[3], AND GUANQUN SU[4]
[1]Department of Aviation Engineering, Inner Mongolia University of Technology, Hohhot 010051, China
[2]School of Electrical Engineering, University of New South Wales (UNSW), Sydney, NSW 4032, Australia
[3]Department of Theoretical Mechanics, Inner Mongolia University of Technology, Hohhot 010051, China
[4]College of Electronic Information Engineering, Inner Mongolia University, Hohhot 010021, China

Corresponding author: Changchun Bao (changchun@imut.edu.cn)

ABSTRACT In this paper, an advanced control method is proposed for a fixed-wing unmanned aerial vehicle (UAV) to maintain the stabilization of its altitude, attitude, and velocity. The mathematical model of a fixed-wing UAV is very complicated because of its characteristics of nonlinearity and large extent of multi-variable coupling. Thus, to design the relevant controller is also difficult. In addition, during the operation of a fixed-wing UAV, the concomitant various uncertainties and disturbances will make the control process harder to accomplish. To solve these problems, this study designs a variable-structure controller with multiple algorithm fusion. The design mainly adopts the backstepping sliding mode control method to simplify the complex nonlinear mathematical model, and an adaptive law is introduced to estimate the uncertainty and disturbance of the system. Subsequently, the tracking error of the controller is proved to converge to zero using Lyapunov's second method. Finally, it is verified that the controller has the ability to stably control a fixed-wing UAV by numerical simulation and can overcome the disturbance and uncertainty. The buffeting also can be eliminated by the adaptive law.

INDEX TERMS Fixed-wing UAVs, adaptive law, backstepping sliding control, uncertainty, disturbance, buffeting phenomenon.

I. INTRODUCTION

Recently, the issue of unmanned aerial vehicles (UAVs) has become an increasingly popular topic. Until now, this technology has played an irreplaceable role in both military and civil applications [1]. Currently, UAVs are mainly divided into two categories: multirotor UAVs and fixed-wing UAVs. Both categories are widely used in different fields, according to their different characteristics. The multirotor UAVs mainly includes quadrotor and crossover twin-rotor UAVs. Quadrotor UAVs are mainly used to complete some tasks with high requirements for maintaining attitude, altitude and position, such as detailed terrain exploration and short-range transportation of small weight materials. This is because of their small size, flexible attitude, and the ability of hover. However, the limitations of airspeed and altitude exist. Crossover twin-rotor UAVs are mostly used to accurately drop heavy loads because of their special physical structure. Their carrying capacity is much stronger than that of quad-rotor UAVs, but they also have flight speed and altitude limitations. Fixed-wing UAVs are aircraft driven by aerodynamic forces acting on a fixed surface, which are often used to accomplish tasks that require high altitude and high speed because of their fast flight speed, long flight distance and strong load capacity characteristics.

Although fixed-wing UAVs have many advantages, designing control systems to ensure good performance is not an easy task. This is because accurate models are needed in the design of controllers, but the models of fixed-wing UAVs are very complex owing to the uncertainty, nonlinearity, and coupling of multiple state quantities. Extensive research has been conducted on the modeling process of fixed-wing UAVs [2], [3], but all of them can only work out approximate mathematical and dynamic models. When the fixed-wing UAV are analysed, it is necessary to make a lot of assumptions in advance, such as taking the UAV as rigid body

The associate editor coordinating the review of this manuscript and approving it for publication was Bidyadhar Subudhi.

and the constant ground acceleration, etc. This is that makes the difference between the actual model and the ideal model, which is also the main reason for the uncertainty of system parameters.

To date, the most common control method for fixed-wing UAVs is the traditional PID control. PID control algorithm has the superior characteristics of simple control principle, easy to modify parameters and low requirements for model accuracy. However, this algorithm has high requirements on the selection of control parameters, which requires a large amount of data experimental testing. Due to the uncertainty in the system, the control parameters obtained by numerical simulation are not always feasible in the actual situation. Thus, a lot of practical experiments are inescapable to optimize the control parameters. This is a complicated and lengthy process. Furthermore, the system of fixed-wing UAVs is a complex nonlinear system, which cannot be directly controlled by traditional PID without a tedious linearization process.

Owing to the significant complexity of the linearization process, to control the fixed-wing UAV accurately, some robust nonlinear control methods can be introduced to avoid the linearization process. The current popular robust control methods include adaptive control [4], [5], neural control [6], linear quadratic control (LQR) [7], linear tracking control [8], dynamic inversion control [9], nested saturation control [10], [11], feedback linearization control [12], [13], backstepping technique [14]–[16], Sliding mode variable structure control [16], [17], etc.

Sliding mode variable structure control is currently one of the mainstream robust control laws, which is mainly aimed at solving the control problem of nonlinear models. The fundamental difference between it and conventional control lies in the discontinuity of control, which means that the switching characteristics of the system structure will change with time. Sliding mode motion can force the system to move up and down with a small amplitude and high frequency along the specified state trajectory under certain characteristics. However, this principle also directly brings the chattering to the system. This phenomenon refers to that the controlled system will vibrate around the sliding surface rather than directly stopping on the surface when it operates under the action of the control law. It poses risks to the stability of the system. At present, how to overcome the chattering problem has become the focus of many scholars.

Several studies have proposed variations in the related aircraft control. Zhang *et al.* [18] introduced an adaptive gain sliding mode control scheme based on a multivariable finite-time observer for a fixed-wing unmanned aircraft (UAV) with unmeasured angular velocity and unknown mismatched disturbances. For the attitude subsystem, a multivariable finite-time observer (MFO) was constructed to estimate the unknown state. Using the estimates provided by the MFO, a new adaptive dual-layer continuous terminal sliding mode (ADL-CTSM) controller was proposed to track the reference attitude instructions in a limited time. The experimental results indicate that the controller can effectively eliminate chattering without a known interference boundary and has good control performance. Espinoza *et al.* [19] designed several backstepping sliding mode controllers, including a backstepping sliding mode controller, backstepping double sliding mode controller, and backstepping high-order sliding mode control (HOSM), to solve the attitude control problem of fixed-wing UAVs and compared their control performance. The experimental data proved that the HOSM has the best performance and can effectively suppress chattering. Castañeda *et al.* [20] provided robust second-order adaptive sliding mode controllers for the attitude and airspeed of fixed-wing UAVs. The controllers could approach the control targets without overestimating the control gain and the known upper bound of the disturbance. The good performance of resisting disturbances and overcoming uncertainty was verified experimentally. The experimental results showed that these controllers can complete the control work well and require less control effort in a limited time. Melkou *et al.* [21] improved the second-order sliding mode control and achieved maintenance control of the altitude and attitude of a fixed-wing UAV. The stability and effectiveness of the controller were also proved by experiments, and the related gain adaptation laws reduced the tremor. Qiu *et al.* [22] presented a quality-driven fixed-wing UAV rather than a traditional aerodynamic-driven UAV and controlled it using a method based on adaptive sliding mode control. The designed controller is a type of adaptive sliding mode controller that integrates a fuzzy system, an RBF neural network, and sliding mode control. The experiments showed that the controller is robust and effective. Wu *et al.* [23] addressed the problem of fixed-wing UAV control by designing a nonsingular fast terminal sliding mode control law. Singularity was avoided by obtaining a modified saturation function near zero. Three different states of moving objects were used for numerical simulation. The simulation results verified the finite-time convergence and stability of the controller. Wang *et al.* [24] proposed a new distributed sliding mode control law to overcome the difficulty of master-slave formation flight with velocity constraints. Driven by the designed control law, the desired formation was achieved, and the linear and angular velocity constraints of the UAV were satisfied. Finally, the results were verified using a numerical simulation. Yang *et al.* [25] proposed a multivariable time-sliding mode interference observer for UAV attitude and airspeed control problems. A new vector control structure was proposed that extended the traditional three-channel vector control. The experiment proved the robustness and stability of this method. Zheng *et al.* [26] solved the control problem of the relative motion model of a fixed-wing UAV aircraft carrier landing using a backstepping sliding mode controller. According to the underactuated characteristics of the two vehicles, the six DOFs of the model were simplified to four DOFs for control. An adaptive backstepping sliding mode controller was used to control the UAV to track the expected landing international and maintain a constant support and roll

angle. These experiments support the feasibility and effectiveness of the proposed method. Jiang *et al.* [27] applied an adaptive inverse sliding mode controller to accomplish the attitude and position control process of a six-degree-of-freedom quadrotor UAV. Internal and external disturbances were estimated using adaptive laws and compensated for the system. Fusion backstepping sliding mode control reduced the requirement of the traditional six-rotor controller design for an accurate model and upper bound of the disturbance. The experiment claimed that the method can effectively and stably complete the control process of a quadrotor UAV.

In this study, a control method combining adaptive method and backstepping sliding modes is proposed to control a fixed-wing UAV. Compared with the existing sliding mode control algorithms, this algorithm can solve the chattering problem while overcoming the uncertainties of model parameters and external disturbances. Because the fixed-wing UAV often works in a state of high moving speed, the precise control of its displacement is of little significance. This design mainly involves the control design of the UAV's attitude, altitude, and flight speed. The dynamic and mathematical models of fixed-wing UAVs are extremely complex. To make it closer to a real situation, it is necessary to consider the coupling effect between different variables. In the controller design process, the part of strong coupling should be carefully analyzed and decoupled, and the controller should be designed for different state variables. The adaptive law is used to estimate the uncertainties and external disturbances of the system and compensate them to the system. In other words, the introduction of adaptive law can help the controller maintain good control performance even when the parameters of the controlled system vary owing to uncertainties. Furthermore, the adaptive law can also be used to eliminate the chattering. The backstepping design method decomposes the complex nonlinear system into subsystems that do not exceed the order of the system, and then introduces the Lyapunov function and the intermediate virtual control for the subsystems. This method is very effective in solving the complex model control problem of fixed-wing UAVs. In this study, the adaptive, backstepping, and sliding mode methods were combined to design the controllers for a fixed-wing UAV.

The remainder of this paper is organized as follows: Section II introduces the kinematics model and dynamics model of fixed-wing UAVs. Section III presents the design of the adaptive backstepping sliding mode control laws and analyzes their stability. Section IV simulates the control system using the MATLAB software. The conclusions are presented in section V.

II. ESTABLISHMENT OF UAV MATHEMATICAL MODEL

Owing to the complexity of the movement of the fixed-wing UAV, the following assumptions are required before the establishment of the dynamics and kinematics models [28], [29].

① The rotation of the earth is stagnant, and the curvature of the earth is zero.

② The body of a fixed-wing UAV is considered rigid and does not deform or vibrate owing to changes in the forces.

③ The drone fuselage was perfectly symmetrical with respect to the central axis plane.

A. MULTIPLE COORDINATE SYSTEM ESTABLISHMENT

A total of 12 state variables were required for the force and motion description of a fixed-wing UAV. There are three displacement state variables with their velocity state variables and three angle state variables with their angular velocity state variables. These 12 state quantities cannot be obtained from a single coordinate system; therefore, it is necessary to establish the following auxiliary coordinate system [28], [29]:

① Ground inertial coordinate system ($O_GX_GY_GZ_G$): The starting position of the UAV is the origin of coordinates, with the X_G-axis pointing to the north, the Y_G-axis pointing to the east, and the Z_G-axis pointing to the Earth's core.

② Body inertial coordinate system ($O_{Bi}X_{Bi}Y_{Bi}Z_{Bi}$): The origin is the center of mass of the UAV, while the X_{Bi}-axis, Y_{Bi}-axis, and Z_{Bi}-axis are parallel to the ground inertial coordinate system and point to due north, due east, and the Earth's core, respectively.

③ Body coordinate system ($O_BX_BY_BZ_B$): The center of mass of the UAV is the origin of the coordinate system, with X_B-axis pointing to the nose, Y_B-axis pointing to the belly, and Z_B-axis pointing to the right wing.

④ Stable coordinate system ($O_SX_SY_SZ_S$): The center of mass of the UAV is the origin, while the X_S-axis points to the direction of the projection of the motion vector of the UAV in the longitudinal symmetric plane, the Z_S-axis points to the right wing of the UAV, and the Y_S-axis is determined by the right-hand rule.

⑤ Airflow coordinate system ($O_AX_AY_AZ_A$): The origin is the center of gravity of the UAV, and the X_A-axis points to the direction of the UAV's motion speed. The Z_A-axis is vertically downward with the X_A-axis in the longitudinal symmetric plane of the UAV, and the Y_A-axis is determined by the right-hand rule.

By designing the transformation matrix according to Ψ, θ, Φ, α, and β, the relationship between the coordinate systems can be determined. Ψ is the yaw angle, θ is the pitch angle, Φ is the roll angle, α is the attack angle, and β is the sideslip angle.

According to these angles, the transformation matrix can be established as follows [30]:

The transformation matrix between $O_{Bi}X_{Bi}Y_{Bi}Z_{Bi}$ and $O_BX_BY_BZ_B$ is as (1), shown at the bottom of the next page.

The transformation matrix between $O_BX_BY_BZ_B$ and $O_AX_AY_AZ_A$ is

$$O_AX_AY_AZ_A = \begin{pmatrix} cos\beta\cos\alpha & \sin\beta & \cos\beta\sin\alpha \\ -sin\beta cos\alpha & cos\beta & -sin\beta\sin\alpha \\ -\sin\alpha & 0 & cos\alpha \end{pmatrix} * (O_BX_BY_BZ_B) \quad (2)$$

B. DYNAMICS MODEL AND KINEMATICS MODEL

It is necessary to determine the definitions of the 12 state quantities of the UAVs. These 12 state variables were defined in terms of the ground coordinate system ($O_GX_GY_GZ_G$). P_x, P_y, P_z are the displacement states of the three axes. u, v, w represent the velocity of the displacement along the three axes. The Euler angle (Ψ, θ, Φ) is the angle at which the UAV body rotates on three axes, and their rate of change is denoted by p, q, r.

Through the transformation matrix established in Section 2.2, the kinematics model of the fixed-wing UAV can be easily obtained [30]. (3) and (4), as shown at the bottom of the page.

In the process of establishing the dynamic model, the calculation is carried out mainly according to Newton's second law. The core formulae are as follows:

$$F = \frac{d}{dt}mV \tag{5}$$

$$M = \frac{d}{dt}H \tag{6}$$

where F is the accumulation of external forces,
m is the mass of UAV,
M is the accumulation of torques,
H is the angular momentum.

By expanding these two formulas according to the characteristics of the fixed-wing UAV, the dynamic model can be obtained as follows [29], [30]:

$$\begin{pmatrix} \dot{u} \\ \dot{v} \\ \dot{w} \end{pmatrix} = \begin{pmatrix} -qw + rv \\ -ru + pw \\ -pv + qu \end{pmatrix} + \frac{1}{m}\begin{pmatrix} f_x \\ f_y \\ f_z \end{pmatrix} \tag{7}$$

where f_x, f_y, f_z are the forces of the UAV along the axis in the ground coordinate system.

$$\begin{pmatrix} \dot{p} \\ \dot{q} \\ \dot{r} \end{pmatrix} = \begin{pmatrix} T_1pq - T_2qr + T_3t_1 + T_4t_3 \\ T_5pr - T_6(p^2 - r^2) + \frac{1}{j_y}t_2 \\ T_7pq - T_1qr + T_4t_1 + T_8t_3 \end{pmatrix} \tag{8}$$

where t_1, t_2, t_3 are the projections of the torque on the three axes in the body coordinate system,

$$j_x = \int \left(z^2 + y^2\right) dm, \quad j_y = \int \left(z^2 + x^2\right) dm,$$

$$j_z = \int (y^2 + x^2) dm, \quad j_{xy} = \int xydm,$$

$$j_{xz} = \int xzdm, \quad j_{yz} = \int yzdm,$$

$$T = j_xj_y - j_{xz}^2, \quad T_1 = \frac{j_{xz}(j_x - j_y + j_z)}{T},$$

$$T_2 = \frac{j_z(j_z - j_y) + j_{xz}^2}{T}, \quad T_3 = \frac{j_z}{T}, \quad T_4 = \frac{j_{xz}}{T},$$

$$T_5 = \frac{j_z - j_x}{j_z}, \quad T_6 = \frac{j_{xz}}{j_y},$$

$$T_7 = \frac{j_x(j_x - j_y) + j_{xz}^2}{T}, \quad T_8 = \frac{j_x}{T}.$$

C. AERODYNAMIC MODEL AND THRUST MODEL

1) ESTABLISHMENT OF AERODYNAMIC MODEL

When the UAV moves relative to the airflow, the aerodynamic force and torque of the UAV will be affected to some extent. The relevant aerodynamics and torques were analyzed from both the longitudinal and lateral perspectives.

According to the longitudinal symmetry plane analysis, the influence of aerodynamics is mainly reflected in the lift force (f_{up}), drag force (f_r) and moment of inertia of rotation around the vector pointing to the wing (t_1) [30].

$$f_{up} = \frac{1}{2}\rho V_a^2 SC_L(\alpha, q, U_1) \tag{9}$$

$$f_r = \frac{1}{2}\rho V_a^2 SC_D(\alpha, q, U_1) \tag{10}$$

$$t_2 = \frac{1}{2}\rho V_a^2 ScC_m(\alpha, q, U_1) \tag{11}$$

where c is the average aerodynamic chord length, ρ is the air density, S is the UAV wing area, C_L is the lift coefficient, C_D is the drag coefficient, C_m is the moment coefficient, U_1 is the elevator command signal.

In the control process of a fixed-wing UAV, the angle of attack is usually very small, so the aerodynamic parameters mentioned above can be regarded as linear. The following results were obtained using the first-order Taylor formula:

$$f_{up} = \frac{1}{2}\rho V_a^2 S(C_L(\alpha) + C_{Lq}\frac{c}{2V_a}q + C_{LU_1}U_1) \tag{12}$$

$$O_BX_BY_BZ_B = \begin{pmatrix} cos\theta\cos\Psi & cos\theta\sin\Psi & -sin\theta \\ sin\Phi sin\theta\cos\Psi - cos\Phi\sin\Psi & sin\Phi sin\theta\sin\Psi + cos\Phi\cos\Psi & sin\Phi\cos\theta \\ cos\Phi sin\theta cos\Psi + sin\Phi\sin\Psi & cos\Phi sin\theta cos\Psi - sin\theta\cos\Psi & cos\Phi\cos\theta \end{pmatrix} * (O_{Bi}X_{Bi}Y_{Bi}Z_{Bi}) \tag{1}$$

$$\begin{pmatrix} \dot{P}_x \\ \dot{P}_y \\ \dot{P}_z \end{pmatrix} = \begin{pmatrix} \cos\Psi cos\theta & \sin\Psi cos\theta & -sin\theta \\ -cos\Phi\sin\Psi + sin\Phi sin\theta\cos\Psi & cos\Phi\cos\Psi + sin\Phi sin\theta\sin\Psi & \cos\theta sin\Phi \\ sin\Phi\sin\Psi + cos\Phi sin\theta cos\Psi & -sin\theta\cos\Psi + cos\Phi sin\theta cos\Psi & \cos\theta cos\Phi \end{pmatrix}^T \begin{pmatrix} u \\ v \\ w \end{pmatrix} \tag{3}$$

$$\begin{pmatrix} \dot{\Psi} \\ \dot{\theta} \\ \dot{\Phi} \end{pmatrix} = \begin{pmatrix} 1 & sin\Phi\tan\theta & cos\Phi\tan\theta \\ 0 & cos\Phi & -sin\Phi \\ 0 & sin\Phi\sec\theta & cos\Phi\sec\theta \end{pmatrix} \begin{pmatrix} p \\ q \\ r \end{pmatrix} \tag{4}$$

$$f_r = \frac{1}{2}\rho V_a^2 S(C_D(\alpha) + C_{Dq}\frac{c}{2V_a}q + C_{DU_1}U_1) \quad (13)$$

$$t_2 = \frac{1}{2}\rho V_a^2 Sc(C_{t_2}(\alpha) + C_{t_2q}\frac{c}{2V_a}q + C_{t_2U_1}U_1) \quad (14)$$

where $C_L(\alpha)$, $C_D(\alpha)$, $C_{t_2}(\alpha)$ are nonlinear equations related to α with different coefficients, $C_{Lq} \triangleq \frac{\partial C_L}{\partial q}$, $C_{LU_1} \triangleq \frac{\partial C_L}{\partial U_1}$, $C_{Dq} \triangleq \frac{\partial C_D}{\partial q}$, $C_{LU_1} \triangleq \frac{\partial C_D}{\partial U_1}$, $C_{t_2q} \triangleq \frac{\partial C_{t_2}}{\partial q}$, $C_{t_2U_1} \triangleq \frac{\partial C_{t_2}}{\partial U_1}$.

The above results (f_{up} *and* f_r) are discussed in the stable coordinate system, and the transformation of these results to the body coordinate system is as (15), shown at the bottom of the page.

According to the analysis of the lateral symmetry plane, the influence of aerodynamics is mainly related to the rudder (U_2), aileron steering gear (U_3), yaw angular velocity (p), roll angular velocity (r) and sideslip angle (β). Their relationship is as follows [31]:

$$f_y = \frac{1}{2}\rho V_a^2 SC_Y(\beta, p, r, U_2, U_3) \quad (16)$$

$$t_1 = \frac{1}{2}\rho V_a^2 SbC_{t_1}(\beta, p, r, U_2, U_3) \quad (17)$$

$$t_3 = \frac{1}{2}\rho V_a^2 SbC_{t_3}(\beta, p, r, U_2, U_3) \quad (18)$$

where C_Y is the dimensionless lateral force coefficient, C_{t_1} is the dimensionless rolling moment coefficient, C_{t_3} is the dimensionless yaw moment coefficient.

Using a method similar to the longitudinal aerodynamic study, the following results can be obtained by the first-order Taylor formula expansion:

$$f_y = \frac{1}{2}\rho V_a^2 S(C_{Y_0} + C_{Y_\beta}\beta + C_{Y_p}\frac{b}{2V_a}p + C_{Y_r}\frac{b}{2V_a}r + C_{YU_2}U_2 + C_{YU_3}U_3) \quad (19)$$

$$t_1 = \frac{1}{2}\rho V_a^2 Sb(C_{t_{1_0}} + C_{t_{1_\beta}}\beta + C_{t_{1_p}}\frac{b}{2V_a}p + C_{t_{1_r}}\frac{b}{2V_a}r + C_{t_1U_2}U_2 + C_{t_1U_3}U_3) \quad (20)$$

$$t_3 = \frac{1}{2}\rho V_a^2 Sb(C_{t_{3_0}} + C_{t_{3_\beta}}\beta + C_{t_{3_p}}\frac{b}{2V_a}p + C_{t_{3_r}}\frac{b}{2V_a}r + C_{t_3U_2}U_2 + C_{t_3U_3}U_3) \quad (21)$$

2) ESTABLISHMENT OF THRUST MODEL

Through force analysis of the propeller used in a fixed-wing UAV [32], the expression of thrust can be obtained as

$$F = \frac{1}{2}\rho S_p C_p\left[(k_m U_4)^2 - V_a^2\right] \quad (22)$$

where S_p is the area swept by the propeller, C_p is the thruster-related parameter, k_m is the propeller engine parameters, U_4 is the propeller engine acceleration.

D. COUPLING OF KINEMATIC AND DYNAMIC MODELS WITH AERODYNAMIC AND THRUST MODELS

By coupling the calculated aerodynamic model, torque model and thrust model with the state equations, the following twelve new state equations can be obtained.

$$\dot{P}_x = \cos\Psi cos\theta u + (-cos\Phi\sin\Psi + sin\Phi sin\theta\cos\Psi + cos\Phi sin\theta cos\Psi)w \quad (23)$$

$$\dot{P}_y = \sin\Psi cos\theta u + (cos\Phi\cos\Psi + sin\Phi sin\theta\sin\Psi)v + (-sin\theta\cos\Psi + cos\Phi sin\theta cos\Psi)w \quad (24)$$

$$\dot{P}_z = sin\theta u - \cos\theta sin\Phi v - \cos\theta cos\Phi w \quad (25)$$

$$\dot{\Psi} = sin\Phi\sec\theta q + cos\Phi\sec\theta r \quad (26)$$

$$\dot{\theta} = cos\Phi q - sin\Phi r \quad (27)$$

$$\dot{\Phi} = p + sin\Phi\tan\theta q + cos\Phi\tan\theta r \quad (28)$$

$$\dot{u} = rv - qw - gsin\theta + \frac{1}{2m}\rho V_a^2 S \times\left[C_1(\alpha) + C_2(\alpha)\frac{cq}{2V_a} + C_3(\alpha)U_1\right] + \frac{1}{2m}\rho S_p C_p\left[(k_m U_4)^2 - V_a^2\right] \quad (29)$$

$$\dot{v} = -ru + pw + gcos\theta sin\Phi + \frac{1}{2m}\rho V_a^2 S\left[C_{Y_0} + C_{Y_\beta}\beta + C_{Y_p}\frac{bp}{2V_a} + C_{Y_r}\frac{br}{2V_a} + C_{YU_2}U_2 + C_{YU_3}U_3\right] \quad (30)$$

$$\dot{w} = -pv + qu + gcos\theta\sin\Phi + \frac{1}{2m}\rho V_a^2 S \times\left[C_4(\alpha) + C_5(\alpha)\frac{cq}{2V_a} + C_6(\alpha)U_1\right] \quad (31)$$

$$\dot{p} = T_1 pq - T_2 qr + \frac{1}{2}\rho V_a^2 Sb(C_7 + C_8\beta + C_9\frac{b}{2V_a}p + C_{10}\frac{b}{2V_a}r + C_{11}U_2 + C_{12}U_3) \quad (32)$$

$$\dot{q} = T_5 pr - T_6(p^2 - r^2) + \frac{1}{2j_y}\rho V_a^2 Sc(C_{t_2}(\alpha) + C_{t_2q}\frac{c}{2V_a}q + C_{t_2U_1}U_1) \quad (33)$$

$$\dot{r} = T_7 pq - T_1 qr + \frac{1}{2}\rho V_a^2 Sb(C_{13} + C_{14}\beta + C_{15}\frac{b}{2V_a}p + C_{16}\frac{b}{2V_a}r + C_{17}U_2 + C_{18}U_3) \quad (34)$$

$$\begin{pmatrix} f_x \\ f_z \end{pmatrix} = \begin{pmatrix} cos\alpha & -sin\alpha \\ sin\alpha & cos\alpha \end{pmatrix}\begin{pmatrix} -f_{up} \\ -f_r \end{pmatrix} = \frac{1}{2}\rho V_a^2 S\begin{pmatrix} [C_L(\alpha)sin\alpha - C_D(\alpha)cos\alpha] + \left[C_{Lq}sin\alpha - C_{Dq}cos\alpha\right]\frac{c}{2V_a}q + \left[C_{LU_1}sin\alpha - C_{DU_1}cos\alpha\right] \\ [-C_L(\alpha)cos\alpha - C_D(\alpha)sin\alpha] + \left[-C_{Dq}sin\alpha - C_{Lq}cos\alpha\right]\frac{c}{2V_a}q + \left[-C_{LU_1}cos\alpha - C_{DU_1}sin\alpha\right] \end{pmatrix} \quad (15)$$

where

$$C_1(\alpha) \triangleq C_L(\alpha)sin\alpha - C_D(\alpha)cos\alpha,$$
$$C_2(\alpha) \triangleq C_{Lq}sin\alpha - C_{Dq}cos\alpha,$$
$$C_3(\alpha) \triangleq C_{LU_1}sin\alpha - C_{DU_1}cos\alpha,$$
$$C_4(\alpha) \triangleq -C_L(\alpha)cos\alpha - C_D(\alpha)sin\alpha,$$
$$C_5(\alpha) \triangleq -C_{Dq}sin\alpha - C_{Lq}cos\alpha,$$
$$C_6(\alpha) \triangleq -C_{LU_1}cos\alpha - C_{DU_1}sin\alpha,$$
$$C_7 = T_3C_{t_{1_0}} + T_4C_{t_{3_0}}, \quad C_8 = T_3C_{t_{1_\beta}} + T_4C_{t_{3_\beta}},$$
$$C_9 = T_3C_{t_{1_p}} + T_4C_{t_{3_p}}, \quad C_{10} = T_3C_{t_{1_r}} + T_4C_{t_{3_r}},$$
$$C_{11} = T_3C_{t_1U_1} + T_4C_{t_3U_1}, \quad C_{12} = T_3C_{t_1U_2} + T_4C_{t_3U_2},$$
$$C_{13} = T_4C_{t_{1_0}} + T_8C_{t_{3_0}}, \quad C_{14} = T_4C_{t_{1_\beta}} + T_8C_{t_{3_\beta}},$$
$$C_{15} = T_4C_{t_{1_p}} + T_8C_{t_{3_p}}, \quad C_{16} = T_4C_{t_{1_r}} + T_8C_{t_{3_r}},$$
$$C_{17} = T_4C_{t_1U_1} + T_8C_{t_3U_1}, \quad C_{18} = T_4C_{t_1U_2} + T_8C_{t_3U_2}.$$

III. ADAPTIVE BACKSTEPPING SLIDING MODE CONTROL LAW DESIGN

The control law designed based on adaptive backstepping sliding mode control can solve the unknown uncertain problem of fixed-wing UAVs, including the uncertainty of the system itself and external disturbances [33], [34]. The adaptive law is used to estimate the uncertainty of the system itself and the external disturbance. Then, the estimated value is compensated to the controller to realize the process of compensate. The existing adaptive backstepping sliding mode control mainly uses self-use law to overcome uncertainty and external disturbance. In this paper, the adaptive law is proposed to accomplish the above task and overcome the impact of chattering at the same time.

Before introducing specific controllers, the control system of fixed-wing UAV is designed as shown in Fig. 1.

The target attitude angle, airspeed and altitude are respectively fed to attitude controller, airspeed controller and altitude solver module at first. Attitude control is mainly accomplished by attitude backstepping sliding mode controller. The attitude adaptive module provides adaptive compensation for the attitude backstepping sliding mode controller by dealing with parameter uncertainty, external disturbance and the chattering caused by controller. The controller output the elevator command signal ($\boldsymbol{U_1}$), rudder ($\boldsymbol{U_2}$), and aileron steering gear ($\boldsymbol{U_3}$) to actuators and collect the attitude feedback to accomplish attitude control.

Airspeed control is mainly accomplished by airspeed inversion sliding mode controller. Its principle is similar to attitude control. The altitude control mainly relies on a PID controller coupled with attitude controller. The altitude solver obtains the desired attitude angles by processing the command height signal and outputs them to the attitude controller. This part will be explained detailly in II.C.

For the fixed-wing UAV controller, this section mentions five related control laws, which include three attitude angle control laws, a flight speed control law, and a flight altitude control law. Their stability are analyzed using the Lyapunov stability criterion.

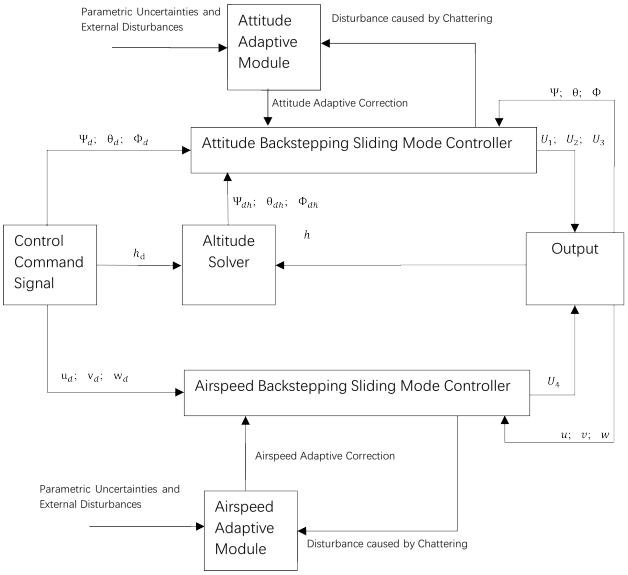

FIGURE 1. Fixed-wing UAV control system.

A. ATTITUDE CONTROLLER DESIGN

The attitude control system includes three angles-θ, Ψ,Φ.

First, it is necessary to obtain the related state-space functions between these angles and the input signal. There are three input signals related to the attitude angle: the elevator command signal (U_1), rudder (U_2), and aileron steering gear (U_3). To establish the required state-space functions, the kinematics and dynamics models need to further handle [35].

For angle Ψ control system,

$$\dot{\Psi} = sin\Phi \sec\theta q + cos\Phi \sec\theta r \tag{35}$$

When the drone is flying, the values of Φ and θ are usual extremely small. The change in angle Ψ is mainly related to r. Therefore, when Ψ is analyzed, we can assume as follows:

$$sin\Phi \approx 0, \quad cos\Phi \approx 1, \ \sec\theta \approx 1$$

View them as the uncertainty of the system.
So that the equation could be rewrite as

$$\dot{\Psi} = r + (cos\Phi \sec\theta - 1)r + sin\Phi \sec\theta q \tag{36}$$

Define $d_{\Psi 1}$ is the external disturbance.

$$d_{\Psi 1} = (cos\Phi \sec\theta - 1)r + sin\Phi \sec\theta q \tag{37}$$

Therefore

$$\dot{\Psi} = r + d_{\Psi 1} \tag{38}$$

Take the derivative of this with respect to t:

$$\ddot{\Psi} = \dot{r} + \dot{d_{\Psi 1}} \tag{39}$$

Substitute (34) into (39):

$$\ddot{\Psi} = T_7pq - T_1qr + \frac{1}{2}\rho V_a^2 Sb(C_{13} + C_{14}\beta + C_{15}\frac{b}{2V_a}p + C_{16}\frac{b}{2V_a}r + C_{17}U_2 + C_{18}U_3) + \dot{d_{\Psi 1}}$$

$$= T_7pq - T_1qr + \frac{1}{2}\rho V_a^2 Sb(C_{13} + C_{14}\beta + C_{15}\frac{b}{2V_a}p + C_{16}\frac{b}{2V_a}(\dot{\Psi} - d_{\Psi 1}) + C_{17}U_2 + C_{18}U_3) + \dot{d_{\Psi 1}}$$
$$= a_{\Psi 1}\dot{\Psi} + a_{\Psi 2}U_2 + d_\Psi \quad (40)$$

where d_Ψ is the total external disturbance,

$$a_{\Psi 1} = \frac{1}{2}\rho V_a^2 SbC_{16}\frac{b}{2V_a}, \quad a_{\Psi 2} = \frac{1}{2}\rho V_a^2 SbC_{17},$$
$$d_\Psi = T_7pq - T_1qr + \frac{1}{2}\rho V_a^2 Sb(C_{13} + C_{14}\beta + C_{15}\frac{b}{2V_a}p - C_{16}\frac{b}{2V_a}d_{\Psi 1} + C_{18}U_3) + \dot{d_{\Psi 1}}.$$

For angle θ control system,

$$\dot{\theta} = cos\Phi q - sin\Phi r \quad (41)$$

Similarly, because the value of angle Φ is small, the effect of angle Φ on the system can be defined as the uncertainty. At the same time, the value of q is the main factor that leads to a change in θ. Thus, the function of $\dot{\theta}$ can be rewritten as

$$\dot{\theta} = \mathrm{q} + (cos\Phi - 1)\mathrm{q} - sin\Phi r = \mathrm{q} + d_{\theta 1} \quad (42)$$

where $d_{\theta 1}$ is the external disturbance of this system and $d_{\theta 1} = (cos\Phi - 1)\mathrm{q} - sin\Phi r$.

Take the derivative of both sides with respect to t:

$$\ddot{\theta} = \dot{\mathrm{q}} + \dot{d_{\theta 1}} \quad (43)$$

Substitute (33) into (43):

$$\ddot{\theta} = T_5pr - T_6(p^2 - r^2) + \frac{1}{2j_y}\rho V_a^2 Sc(C_{t_2}(\alpha) + C_{t_2 q}\frac{c}{2V_a}q + C_{t_2U_1}U_1) + \dot{d_{\theta 1}} \quad (44)$$

According to [12], $\alpha = \theta - \varepsilon$,where ε is Climbing Angle.

It is already known that $C_{t_2}(\alpha)$ is a nonlinear model related to torque that can only be obtained through wind tunnel flight tests. Therefore, it is feasible to replace it with a linear model -$C_{t_2}(\alpha) = C_{t_{20}} + C_{t_{21}}\alpha$ [3].

Therefore, the function could be written as

$$\ddot{\theta} = T_5pr - T_6(p^2 - r^2) + \frac{1}{2j_y}\rho V_a^2 Sc\{C_{t_{20}} + C_{t_{21}}(\theta - \varepsilon) + C_{t_2 q}\frac{c}{2V_a}q + C_{t_2U_1}U_1\} + \dot{d_{\theta 1}}$$
$$= a_{\theta 1}\dot{\theta} + a_{\theta 2}\theta + a_{\theta 3}U_1 + d_\theta \quad (45)$$

where d_θ is the total external disturbance,

$$a_{\theta 1} = \frac{1}{2j_y}\rho V_a^2 SC_{t_2 q}\frac{\mathrm{C}^2}{2V_a}, \quad a_{\theta 2} = \frac{1}{2j_y}\rho V_a^2 ScC_{t_{21}},$$
$$a_{\theta 3} = \frac{1}{2j_y}\rho V_a^2 ScC_{t_2U_1},$$
$$d_\theta = T_5pr - T_6(p^2 - r^2) + \frac{1}{2j_y}\rho V_a^2 Sc \times (C_{t_{20}} - C_{t_{21}}\varepsilon - C_{t_2 q}\frac{c}{2V_a}d_{\theta 1}) + \dot{d_{\theta 1}}.$$

For angle Φ control system,

$$\dot{\Phi} = p + sin\Phi\tan\theta\mathrm{q} + cos\Phi\tan\theta r \quad (46)$$

Define $d_{\theta 1}$ is the external disturbance of this system. Because of the close-to-zero values of $sin\Phi$, $\tan\theta$ and $cos\Phi$, $d_{\Phi 1} = sin\Phi\tan\theta\mathrm{q} + cos\Phi\tan\theta r$.

$$\dot{\Phi} = p + d_{\Phi 1} \quad (47)$$

The derivation of $\dot{\Phi}$ with respect to t is shown below:

$$\ddot{\Phi} = \dot{p} + \dot{d_{\Phi 1}} \quad (48)$$

Substitute (32) into (48):

$$\ddot{\Phi} = T_1pq - T_2qr + \frac{1}{2}\rho V_a^2 Sb(C_7 + C_8\beta + C_9\frac{b}{2V_a}p + C_{10}\frac{b}{2V_a}r + C_{11}U_2 + C_{12}U_3) + \dot{d_{\Phi 1}}$$
$$= a_{\Phi 1}\dot{\Phi} + a_{\Phi 2}U_3 + d_\Phi \quad (49)$$

where d_θ is total external disturbance of this system,

$$a_{\Phi 1} = \frac{1}{2}\rho V_a^2 SbC_9\frac{b}{2V_a}, \quad a_{\Phi 2} = \frac{1}{2}\rho V_a^2 SbC_{12},$$
$$d_\Phi = T_1pq - T_2qr + \frac{1}{2}\rho V_a^2 Sb(C_7 + C_8\beta - C_9\frac{b}{2V_a}d_{\theta 1} + C_{10}\frac{b}{2V_a} + C_{11}U_2) + \dot{d_{\Phi 1}}.$$

Therefore, the desired state-space vector of the attitude angle control system can be defined as

$$X = (\Psi, \dot{\Psi}, \theta, \dot{\theta}, \Phi, \dot{\Phi})^T \in R^6 \quad (50)$$

The output vector of this system can be defined as

$$Y = (\Psi, \theta, \Phi)^T \in R^3 \quad (51)$$

Letting $x_1 = \Psi, x_2 = \dot{\Psi}, x_3 = \theta, x_4 = \dot{\theta}, x_5 = \Phi, x_6 = \dot{\Phi}$. The related state-space function can be obtained as

$$\begin{cases} \dot{X} = A(X) + B(X)U = \begin{cases} x_2 \\ a_{\Psi 1}x_2 + a_{\Psi 2}U_2 + d_\Psi \\ x_4 \\ a_{\theta 1}x_4 + a_{\theta 2}x_3 + a_{\theta 3}U_1 + d_\theta \\ x_6 \\ a_{\Phi 1}x_6 + a_{\Phi 2}U_3 + d_\Phi \end{cases} \\ Y = C(X) \end{cases} \quad (52)$$

Second, the adaptive backstepping sliding mode controller can be designed according to the above state-space function.

The yaw angle controller design is based on below state space function group.

$$\begin{cases} \dot{x_1} = x_2 \\ \dot{x_2} = a_{\Psi 1}x_2 + a_{\Psi 2}U_2 + D_\Psi \\ y_1 = x_1 \end{cases} \quad (53)$$

where D_Ψ is the total uncertainty of the yaw angle controller, which can be expressed as

$$D_\Psi = \Delta a_{\psi 1} x_2 + \Delta a_{\psi 2} U_2 + d_\Psi \tag{54}$$

In the process of recursion, the sliding mode surface and adaptive law need to be introduced to determine the control effect of the controller. Adaptive estimation mainly focuses on the design of D_Ψ. There are three significant steps in the design of the adaptive backstepping sliding mode controller.

① The construction of virtual control signal through Lyapunov function and definition of sliding surface.
② The extension of the Lyapunov equation
③ The introduction of adaptive law and control law.

So that, the adaptive backstepping sliding mode control law could be obtained.

Assume x_{1d} is the yaw angle command signal. The design details of the yaw angle controller are presented below.

Step 1:

Define tracking error is $z_{\psi 1} = x_1 - x_{1d}$, so the derivative of tracking error is $\dot{z_{\psi 1}} = \dot{x_1} - \dot{x_{1d}}$.

Establish the Lyapunov function ($V_{\psi 1}$):

$$V_{\psi 1} = \frac{1}{2} z_{\psi 1}^2 \tag{55}$$

We define $x_2 = z_{\psi 2} + \dot{x_{1d}} - c_{\psi 1} z_{\psi 1}$, where $c_{\psi 1}$ is a constant greater than zero and $z_{\psi 2}$ is the virtual control signal.

Then the derivative of $z_{\psi 1}$ can be expressed as

$$\dot{z_{\psi 1}} = x_2 - \dot{x_{1d}} = z_{\psi 2} - c_{\psi 1} z_{\psi 1} \tag{56}$$

The derivative of $V_{\psi 1}$ can be expressed as

$$\dot{V_{\psi 1}} = z_{\psi 1} \dot{z_{\psi 1}} = z_{\psi 1} z_{\psi 2} - c_{\psi 1} z_{\psi 1}^2 \tag{57}$$

The sliding surface is defined below.

$$\tau_\Psi = k_{\psi 1} z_{\psi 1} + z_{\psi 2} \tag{58}$$

where $k_{\psi 1} > 0$.

Substitute (56) into (58):

$$\tau_\Psi = k_{\psi 1} z_{\psi 1} + \dot{z_{\psi 1}} + c_{\psi 1} z_{\psi 1} = (k_{\psi 1} + c_{\psi 1}) z_{\psi 1} + \dot{z_{\psi 1}} \tag{59}$$

It is obvious that $k_{\psi 1} + c_{\psi 1} > 0$. If $\tau_\Psi = 0$, $z_{\psi 1} = 0$ and $z_{\psi 2} = 0$, which, in turn, will lead $\dot{V_{\psi 1}} \leq 0$. Therefore, it is necessary to introduce Step 2.

Step 2:

Establish another Lyapunov function ($V_{\psi 2}$):

$$\begin{aligned} V_{\psi 2} &= V_{\psi 1} + \frac{1}{2} \tau_\Psi^2 \qquad (60) \\ \dot{V_{\psi 2}} &= \dot{V_{\psi 1}} + \tau_\Psi \dot{\tau_\Psi} \\ &= z_{\psi 1} z_{\psi 2} - c_{\psi 1} z_{\psi 1}^2 + \tau_\Psi \dot{\tau_\Psi} \\ &= z_{\psi 1} z_{\psi 2} - c_{\psi 1} z_{\psi 1}^2 + \tau_\Psi \left(k_{\psi 1} \dot{z_{\psi 1}} + \dot{z_{\psi 2}} \right) \\ &= z_{\psi 1} z_{\psi 2} - c_{\psi 1} z_{\psi 1}^2 + \tau_\Psi \\ &\quad \times \left(k_{\psi 1} \left(z_{\psi 2} - c_{\psi 1} z_{\psi 1} \right) + \dot{x_2} - \ddot{x_{1d}} + c_{\psi 1} \dot{z_{\psi 1}} \right) \\ &= z_{\psi 1} z_{\psi 2} - c_{\psi 1} z_{\psi 1}^2 + \tau_\Psi \left(k_{\psi 1} \left(z_{\psi 2} - c_{\psi 1} z_{\psi 1} \right) \right. \\ &\quad \left. + a_{\psi 1} x_2 + a_{\psi 2} U_2 + D_\Psi - \ddot{x_{1d}} + c_{\psi 1} \dot{z_{\psi 1}} \right) \\ &= z_{\psi 1} z_{\psi 2} - c_{\psi 1} z_{\psi 1}^2 \\ &\quad + \tau_\Psi (k_{\psi 1} (z_{\psi 2} - c_{\psi 1} z_{\psi 1}) + a_{\psi 1} (z_{\psi 2} + \dot{x_{1d}} \\ &\quad - c_{\psi 1} z_{\psi 1}) + a_{\psi 2} U_2 + D_\Psi - \ddot{x_{1d}} + c_{\psi 1} \dot{z_{\psi 1}}) \qquad (61) \end{aligned}$$

Because the uncertain part of the system appears in $\dot{V_{\psi 2}}$, Step 3 is required to determine whether $\dot{V_{\psi 2}}$ is greater than zero.

Step 3:

In the sliding mode control process, excellent stability and robustness require a precise upper bound on the total uncertainty. However, in the actual operation of a UAV, the accurate upper bound of the total uncertainty is difficult to obtain. Therefore, an adaptive law is introduced to estimate the upper bound of the total uncertainty of the system.

Establish the third Lyapunov function ($V_{\psi 3}$):

$$V_{\psi 3} = V_{\psi 2} + \frac{1}{2 \delta_\Psi} \widetilde{D_\Psi}^2 \tag{62}$$

where $\widetilde{D_\Psi} = D_\Psi - \widehat{D_\Psi}$ is the error in the estimation of D_Ψ, $\widehat{D_\Psi}$ is the value in the estimation of D_Ψ, δ is a normal number.

$$\dot{V_{\psi 3}} = \dot{V_{\psi 2}} + \frac{1}{\delta_\Psi} \widetilde{D_\Psi} \dot{\widetilde{D_\Psi}} = \dot{V_{\psi 2}} + \frac{1}{\delta_\Psi} \widetilde{D_\Psi} (\dot{D_\Psi} - \dot{\widehat{D_\Psi}}) \tag{63}$$

Due to the insensible change of D_Ψ, assuming $\dot{D_\Psi} = 0$ is feasible.

$$\begin{aligned} \dot{V_{\psi 3}} &= \dot{V_{\psi 2}} - \frac{1}{\delta_\Psi} \widetilde{D_\Psi} \dot{\widehat{D_\Psi}} \\ &= z_{\psi 1} z_{\psi 2} - c_{\psi 1} z_{\psi 1}^2 \\ &\quad + \tau_\Psi \left(k_{\psi 1} \left(z_{\psi 2} - c_{\psi 1} z_{\psi 1} \right) + a_{\psi 1} (z_{\psi 2} + \dot{x_{1d}} \right. \\ &\quad \left. - c_{\psi 1} z_{\psi 1}) + a_{\psi 2} U_2 + D_\Psi - \ddot{x_{1d}} + c_{\psi 1} \dot{z_{\psi 1}} \right) \\ &\quad - \frac{1}{\delta_\Psi} \widetilde{D_\Psi} \dot{\widehat{D_\Psi}} \\ &= z_{\psi 1} z_{\psi 2} - c_{\psi 1} z_{\psi 1}^2 \\ &\quad + \tau_\Psi \left(k_{\psi 1} \left(z_{\psi 2} - c_{\psi 1} z_{\psi 1} \right) + a_{\psi 1} (z_{\psi 2} + \dot{x_{1d}} \right. \\ &\quad \left. - c_{\psi 1} z_{\psi 1}) + a_{\psi 2} U_2 + \widehat{D_\Psi} - \ddot{x_{1d}} + c_{\psi 1} \dot{z_{\psi 1}} \right) \\ &\quad - \frac{1}{\delta_\Psi} \widetilde{D_\Psi} (\dot{\widehat{D_\Psi}} + \delta_\Psi \tau_\Psi) \qquad (64) \end{aligned}$$

Select the yaw angle control law:

$$\begin{aligned} U_2 = -\frac{1}{a_{\Psi 2}} &(-k_{\psi 1} \left(z_{\psi 2} - c_{\psi 1} z_{\psi 1} \right) \\ &- a_{\psi 1} \left(z_{\psi 2} + \dot{x_{1d}} - c_{\psi 1} z_{\psi 1} \right) - \widehat{D_\Psi} \\ &+ \ddot{x_{1d}} - c_{\psi 1} \dot{z_{\psi 1}} - h_{\psi 1} (\tau_\Psi + \varepsilon_\Psi sgn(\tau_\Psi))) \end{aligned} \tag{65}$$

where $h_{\psi 1}$ and ε_Ψ are positive constants.

Design the adaptive law of D_Ψ:

$$\dot{\widehat{D_\Psi}} = -\delta_\Psi \tau_\Psi \tag{66}$$

Similarly, the control laws and adaptive laws of the pitch and roll angles are as follows:

$$U_1 = -\frac{1}{a_{\theta 3}} (-k_{\theta 1} \left(z_{\theta 2} - c_{\theta 1} z_{\theta 1} \right) - a_{\theta 1} (z_{\theta 2} + \dot{x_{3d}} - c_{\theta 1} z_{\theta 1})$$

$$- a_{\theta 2}x_3 - \widehat{D_\theta} + \ddot{x}_{1d} - c_{\theta 1}\dot{z}_{\theta 1} - h_{\theta 1}(\tau_\theta + \varepsilon_\theta sgn(\tau_\theta))) \tag{67}$$

$$\dot{\widehat{D_\theta}} = -\delta_\theta \tau_\theta \tag{68}$$

$$\begin{aligned} U_3 = &-\frac{1}{a_{\Phi 2}}(-k_{\Phi 1}(z_{\Phi 2} - c_{\Phi 1}z_{\Phi 1}) \\ &- a_{\Phi 1}(z_{\Phi 2} + \dot{x}_{5d} - c_{\Phi 1}z_{\Phi 1}) - \widehat{D_\Phi} + \ddot{x}_{5d} \\ &- c_{\Phi 1}\dot{z}_{\Phi 1} - h_{\Phi 1}(\tau_\Phi + \varepsilon_\Phi sgn(\tau_\Phi))) \end{aligned} \tag{69}$$

$$\dot{\widehat{D_\Phi}} = -\delta_\Phi \tau_\Phi \tag{70}$$

where $z_{\theta 1} = x_4 - \dot{x}_{3d} = z_{\theta 2} - c_{\theta 1}z_{\theta 1}$, $z_{\Phi 1} = x_6 - \dot{x}_{5d} = z_{\Phi 2} - c_{\Phi 1}z_{\Phi 1}$, $z_{\theta 2} = x_4 - \dot{x}_{3d} + c_{\theta 1}z_{\theta 1}$, $z_{\Phi 2} = x_6 - \dot{x}_{5d} + c_{\Phi 1}z_{\Phi 1}$, $\tau_\theta = k_{\theta 1}z_{\theta 1} + z_{\theta 2}$, $\tau_\Phi = k_{\Phi 1}z_{\Phi 1} + z_{\Phi 2}$, $c_{\theta 1}, k_{\theta 1}, h_{\theta 1}, \varepsilon_\theta, c_{\Phi 1}, k_{\Phi 1}, h_{\Phi 1}, \varepsilon_\Phi$ are positive constants.

B. AIRSPEED CONTROLLER DESIGN

The airspeed of the UAV is the sum of the three-axis velocity vectors in the body coordinate system.

$$V_a = \sqrt{u^2 + v^2 + w^2} \tag{71}$$

When airspeed control is carried out, the control process can be greatly simplified by only controlling the velocity vector in the direction of the X-axis and treating the velocity vectors in the other two axes as disturbances.

Assume $v = 0$, $w = 0$.

Therefore,

$$V_a = u + d_{V_a 1} \tag{72}$$

where $d_{V_a}1$ is the disturbance of v and w.

Taking derivative V_a:

$$\dot{V}_a = \dot{u} + \dot{d_{V_a 1}} \tag{73}$$

Substituting (29) into (73), it can be obtained as

$$\begin{aligned} \dot{V}_a = &rv - qw - gsin\theta + \frac{1}{2m}\rho V_a^2 S \\ &\times \left[C_1(\alpha) + C_2(\alpha)\frac{cq}{2V_a} + C_3(\alpha)U_1\right] \\ &+ \frac{1}{2m}\rho S_p C_p\left[(k_m U_4)^2 - V_a^2)\right] + \dot{d_{V_a 1}} \end{aligned} \tag{74}$$

According to (74), the conclusion that V_a can be controlled by both the pitch angle (θ) and propeller engine accelerograph (U_4) can be obtained. Here, we choose to use U_4 to control airspeed and regard the influence of the pitch angle as a disturbance.

Therefore, the (74) could be rewritten as

$$\begin{aligned} \dot{V}_a = &\frac{1}{2m}\rho V_a^2 SC_1(\alpha) + \frac{1}{4m}\rho SV_a C_2(\alpha)cq + \frac{1}{2m}\rho V_a^2 \\ &\times SC_3(\alpha)U_1 + \frac{1}{2m}\rho S_p C_p(k_m U_4)^2 \\ &- \frac{1}{2m}\rho S_p C_p V_a^2 + d_{V_a 2} \end{aligned} \tag{75}$$

where $d_{V_a}2 = rv - qw - gsin\theta + \dot{d_{V_a 1}}$.

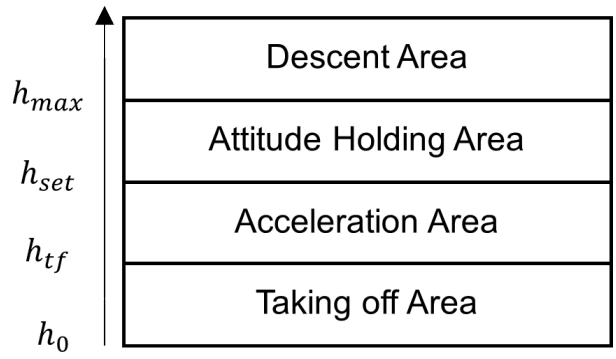

FIGURE 2. Attitude piecewise control diagram.

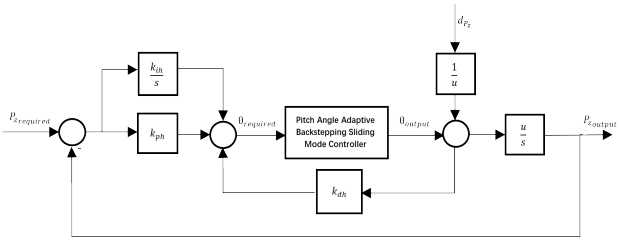

FIGURE 3. Coupled controller.

Taking derivative $\dot{V}_a$:

$$\begin{aligned} \ddot{V}_a = &\frac{1}{m}\rho SC_1(\alpha)V_a + \frac{1}{4m}\rho SC_2(\alpha)cq\dot{V}_a + \frac{1}{m}\rho SC_3(\alpha) \\ &\times U_1 V_a + \frac{1}{m}\rho S_p C_p k_m^2 U_4 - \frac{1}{m}\rho S_p C_p V_a + \dot{d_{V_a 2}} \\ = &a_{V_a 1}V_a + a_{V_a 2}\dot{V}_a + a_{V_a 3}U_4 + \dot{d_{V_a 2}} \end{aligned} \tag{76}$$

where $a_{V_a 1} = \frac{1}{m}\rho SC_1(\alpha) + \frac{1}{m}\rho SC_3(\alpha)U_1 - \frac{1}{m}\rho S_p C_p$, $a_{V_a 2} = \frac{1}{4m}\rho SC_2(\alpha)cq$, $a_{V_a 3} = \frac{1}{m}\rho S_p C_p k_m^2$.

Letting $x_7 = V_a$, $x_8 = \dot{V}_a$, The related state space function could be obtained as

$$\begin{cases} \dot{x_7} = x_8 \\ \dot{x_8} = a_{V_a 1}x_7 + a_{V_a 2}x_8 + a_{V_a 3}U_4 + D_{V_a} \\ y_7 = x_7 \end{cases} \tag{77}$$

where $D_{V_a} = \Delta a_{V_a 1}x_7 + \Delta a_{V_a 2}x_8 + \Delta a_{V_a 3}U_4 + \dot{d_{V_a 2}}$ is the total uncertainty.

Similar to the attitude controller design, the control law and adaptive law of airspeed can be obtained as follows:

$$\begin{aligned} U_4 = &-\frac{1}{a_{V_a 3}}(-k_{V_a 1}\left(z_{V_a 2} - c_{V_a 1}z_{V_a 1}\right) - a_{V_a 2}(z_{V_a 2} + \dot{x_7}_d \\ &- c_{V_a 1}z_{V_a 1}) - a_{V_a 1}x_7 - \widehat{D_{V_a}} + \ddot{x_7}_d - c_{V_a 1}\dot{z}_{V_a 1} \\ &- h_{V_a 1}(\tau_{V_a} + \varepsilon_{V_a}sgn(\tau_{V_a}))) \end{aligned} \tag{78}$$

$$\dot{\widehat{D_{V_a}}} = -\delta_{V_a}\tau_{V_a} \tag{79}$$

where $z_{V_a 1} = x_8 - \dot{x_7}_d = z_{V_a 2} - c_{V_a 1}z_{V_a 1}$, $z_{V_a 2} = x_8 - \dot{x_7}_d + c_{V_a 1}z_{V_a 1}$, $\tau_{V_a} = k_{V_a 1}z_{V_a 1} + z_{V_a 2}$, $\tau_{V_a} = k_{V_a 1}z_{V_a 1} + z_{V_a 2}$, $c_{V_a 1}, k_{V_a 1}, h_{V_a 1}, \varepsilon_{V_a}$ are positive constants.

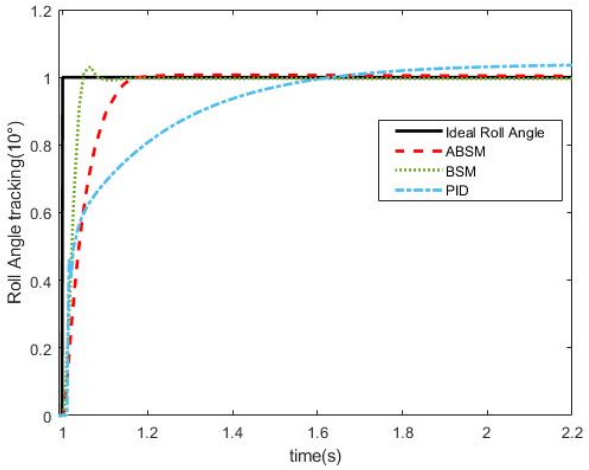

FIGURE 4. Roll angle tracking comparison.

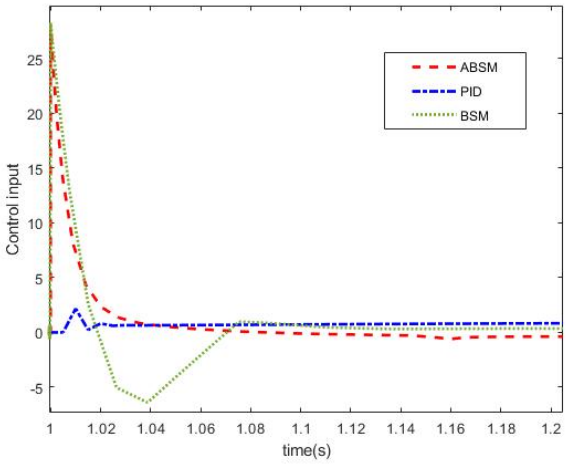

FIGURE 5. Roll angle controllers' input signal comparison.

C. ALTITUDE CONTROLLER DESIGN

The altitude control of a fixed-wing UAV is a relatively more complicated control process. To achieve this, it is necessary to first analyze the equation of state associated with P_z.

$$\dot{P}_z = sin\theta u - \cos\theta sin\Phi v - \cos\theta cos\Phi w \tag{80}$$

In the airspeed control process under ideal conditions, the following assumptions can be made:

$$v = 0, \quad w = 0.$$

According to (80), the flight altitude is mainly related to the pitch angle and airspeed. To simplify the control process, the flight altitude state equation is modified as follows:

$$\begin{aligned}\dot{P}_z &= u\theta + sin\theta u - u\theta - \cos\theta sin\Phi v - \cos\theta cos\Phi w \\ &= u\theta + d_{P_z}\end{aligned} \tag{81}$$

where $d_{P_z} = sin\theta u - u\theta - \cos\theta sin\Phi v - \cos\theta cos\Phi w$ is defined as disturbance.

According to (81), it is known that P_z is determined by u and θ. Because it is complicated to control the flight altitude

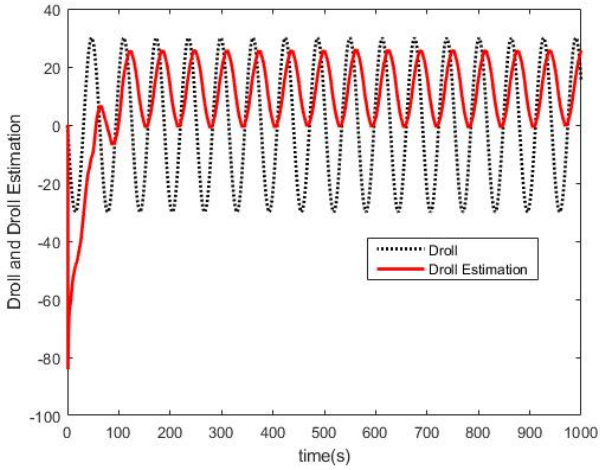

FIGURE 6. Roll angle ABSM controller's adaptive uncertainty estimation signal.

TABLE 1. Control performance indexes of different roll angle controllers.

	PID	BSM	ABSM
Stead error	0.39°	-0.03°	0.05°
Overshoot	0°	0.32°	0°
React time	1.18s	0.19s	0.24s

by using the attitude angle and airspeed at the same time, this section divides the flight process into different stages according to the altitude of the UAV to use different control methods. The altitude control process is mainly divided into four areas: taking off area, acceleration area, attitude holding area, and descent area (shown in Fig.2).

During the UAV takeoff, the fixed throttle opening extent and pitch angle were set to ensure that the UAV stably entered the acceleration zone from the take-off zone. In the acceleration area, the drone's pitch angle is set to a fixed value (h_{tf}), and the propeller engine accelerograph was used to drive the drone up to the command speed and into the altitude-holding zone. Subsequently, in the attitude holding area, a controller coupled with PID control and sliding mode inversion adaptive control is used to adjust the height, which is also the main design target of this section.

Finally, if the height of the UAV exceeds the upper limit of the rated flight height (h_{max}), it enters the descent zone. Within this range, the throttle opening was set to 0, and the coupled altitude controller completed the descent process of the UAV until it reached the command height range.

The UAV airspeed can be regarded as a constant value when the altitude is controlled by the pitch angle.

$$\dot{P}_z = u\theta + d_{P_z} \tag{82}$$

Taking $\dot{P}_z$ Laplace transform, the transfer function can be obtained as

$$P_z(s) = \frac{u}{s}(\theta + \frac{1}{u}d_{P_z}) \tag{83}$$

The coupling controller based on PID control and sliding mode inversion adaptive control can be designed as shown in Fig.3.

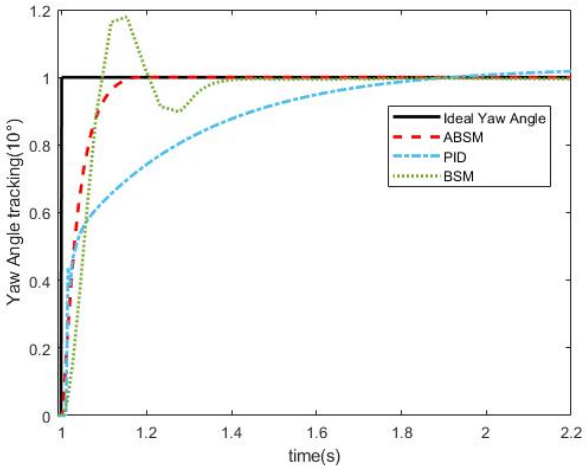

FIGURE 7. Yaw angle tracking comparison.

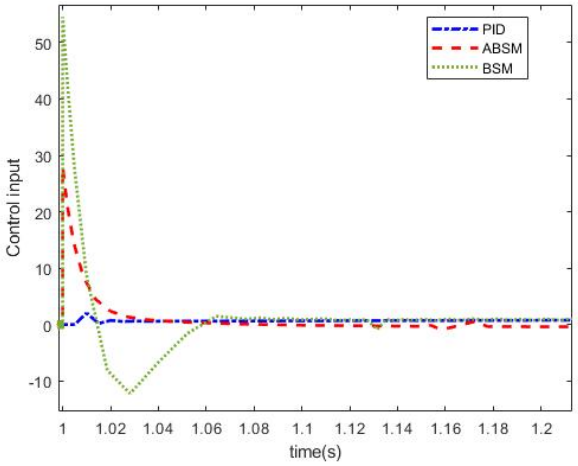

FIGURE 8. Yaw angle controllers' input signal comparison.

The desired pitch angle was calculated through the front end of the PID controller after setting the target altitude. Then, the pitch angle is controlled by the adaptive sliding mode backstepping pitch angle controller designed above. The required pitch angle is returned to the PID controller to achieve altitude control.

D. STABILITY ANALYSIS

In this section, Lyapunov's second method is used to judge the stability of the control system [36]–[38].

Lyapunov'S Second Method: Construct a Lyapunov function according to the system; if the function is positive definite, and the derivative of the function is negative definite, then the system tends to be stable.

Take Yaw Angle controller as an example for analysis:

In the process of designing this controller, three Lyapunov equations were established, which can be expressed as

$$V_{\Psi 1} = \frac{1}{2} z_{\Psi 1}^2 \tag{84}$$

$$V_{\Psi 2} = V_{\Psi 1} + \frac{1}{2} \tau_{\Psi}^2 \tag{85}$$

$$V_{\Psi 3} = V_{\Psi 2} + \frac{1}{2\delta_{\Psi}} \widetilde{D_{\Psi}}^2 \tag{86}$$

By combining them, the total Lyapunov equation can be obtained:

$$V_{\Psi 3} = \frac{1}{2} z_{\Psi 1}^2 + \frac{1}{2} \tau_{\Psi}^2 + \frac{1}{2\delta_{\Psi}} \widetilde{D_{\Psi}}^2 \tag{87}$$

Because δ_{Ψ} is a positive constant, $V_{\Psi 3}$ is obviously positive definite.

Furthermore, whether $\dot{V_{\Psi 3}}$ is negative definite or not needed to be determined.

Substituting (65) and (66) into (64), the derivative of the Lyapunov function can be replaced as follows:

$$\begin{aligned}
\dot{V_{\Psi 3}} &= z_{\Psi 1} z_{\Psi 2} - c_{\Psi 1} z_{\Psi 1}^2 + \tau_{\Psi} k_{\Psi 1} \left(z_{\Psi 2} - c_{\Psi 1} z_{\Psi 1} \right) \\
&\quad + a_{\Psi 1} \left(z_{\Psi 2} + \dot{x_{1d}} - c_{\Psi 1} z_{\Psi 1} \right) \\
&\quad + a_{\Psi 2} \left[-\frac{1}{a_{\Psi 2}} \left(-k_{\Psi 1} \left(z_{\Psi 2} - c_{\Psi 1} z_{\Psi 1} \right) - a_{\Psi 1} \left(z_{\Psi 2} \right. \right. \right. \\
&\quad \left. \left. + \dot{x_{1d}} - c_{\Psi 1} z_{\Psi 1} \right) - \widehat{D_{\Psi}} + \ddot{x_{1d}} - c_{\Psi 1} \dot{z_{\Psi 1}} - h_{\Psi 1} \right. \\
&\quad \left. \left(\tau_{\Psi} + \varepsilon_{\Psi} sgn \left(\tau_{\Psi} \right) \right) \right) \Bigg] \\
&\quad + \widehat{D_{\Psi}} - \ddot{x_{1d}} + c_{\Psi 1} \dot{z_{\Psi 1}} - \frac{1}{\delta_{\Psi}} \widetilde{D_{\Psi}} \left(-\delta_{\Psi} \tau_{\Psi} + \delta_{\Psi} \tau_{\Psi} \right) \\
&= z_{\Psi 1} z_{\Psi 2} - c_{\Psi 1} z_{\Psi 1}^2 - \tau_{\Psi} h_{\Psi 1} \left(\tau_{\Psi} + \varepsilon_{\Psi} sgn \left(\tau_{\Psi} \right) \right) \\
&= z_{\Psi 1} z_{\Psi 2} - c_{\Psi 1} z_{\Psi 1}^2 - h_{\Psi 1} \tau_{\Psi}^2 - h_{\Psi 1} \varepsilon_{\Psi} \left| \tau_{\Psi} \right|
\end{aligned} \tag{88}$$

Take auxiliary matrixes:

$$\boldsymbol{O} = \begin{pmatrix} c_{\Psi 1} + h_{\Psi 1} k_{\Psi 1}^2 & h_{\Psi 1} k_{\Psi 1} - \frac{1}{2} \\ h_{\Psi 1} k_{\Psi 1} - \frac{1}{2} & h_{\Psi 1} \end{pmatrix} \tag{89}$$

$$\boldsymbol{Z} = \begin{pmatrix} z_{\Psi 1} \\ z_{\Psi 2} \end{pmatrix}$$

$$\begin{aligned}
\boldsymbol{Z^T O Z} &= \begin{pmatrix} z_{\Psi 1} & z_{\Psi 2} \end{pmatrix} \begin{pmatrix} c_{\Psi 1} + h_{\Psi 1} k_{\Psi 1}^2 & h_{\Psi 1} k_{\Psi 1} - \frac{1}{2} \\ h_{\Psi 1} k_{\Psi 1} - \frac{1}{2} & h_{\Psi 1} \end{pmatrix} \\
&\quad \times \begin{pmatrix} z_{\Psi 1} \\ z_{\Psi 2} \end{pmatrix} \\
&= c_{\Psi 1} z_{\Psi 1}^2 - z_{\Psi 1} z_{\Psi 2} + h_{\Psi 1} k_{\Psi 1}^2 z_{\Psi 1}^2 \\
&\quad + 2 h_{\Psi 1} k_{\Psi 1} z_{\Psi 1} z_{\Psi 2} + h_{\Psi 1} z_{\Psi 2}^2 \\
&= c_{\Psi 1} z_{\Psi 1}^2 - z_{\Psi 1} z_{\Psi 2} + h_{\Psi 1} \\
&\quad \times \left(k_{\Psi 1}^2 z_{\Psi 1}^2 + 2 k_{\Psi 1} z_{\Psi 1} z_{\Psi 2} + z_{\Psi 2}^2 \right) \\
&= c_{\Psi 1} z_{\Psi 1}^2 - z_{\Psi 1} z_{\Psi 2} + h_{\Psi 1} \left(k_{\Psi 1} z_{\Psi 1} + z_{\Psi 2} \right)^2 \\
&= c_{\Psi 1} z_{\Psi 1}^2 - z_{\Psi 1} z_{\Psi 2} + h_{\Psi 1} \tau_{\Psi}
\end{aligned} \tag{90}$$

Therefore, $\dot{V_{\Psi 3}} = -\boldsymbol{Z^T O Z} - h_{\Psi 1} \varepsilon_{\Psi} \left| \tau_{\Psi} \right|$.

If $\boldsymbol{O}$ is positive definite, $\dot{V_{\Psi 3}}$ will be negative definite.

$$\begin{aligned}
|\boldsymbol{O}| &= h_{\Psi 1} (c_{\Psi 1} + h_{\Psi 1} k_{\Psi 1}^2) - \left(h_{\Psi 1} k_{\Psi 1} - \frac{1}{2} \right)^2 \\
&= h_{\Psi 1} (c_{\Psi 1} + k_{\Psi 1}) - \frac{1}{4}
\end{aligned} \tag{91}$$

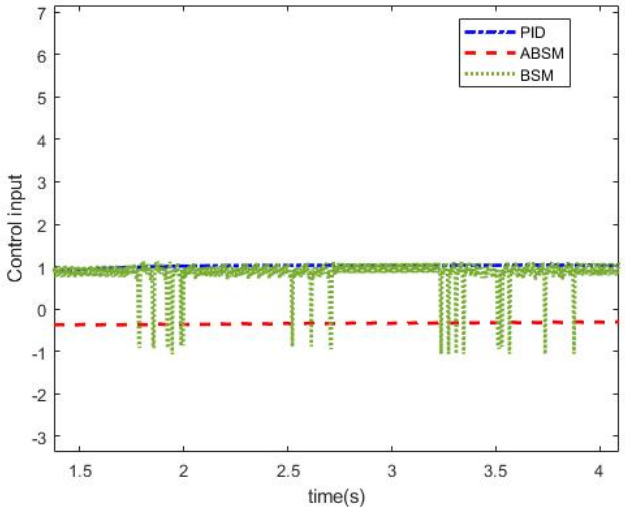

FIGURE 9. Yaw angle controllers' input signal buffeting.

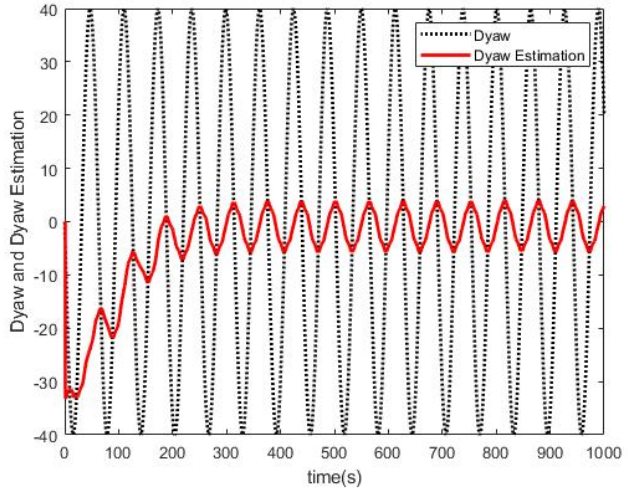

FIGURE 10. Yaw angle ABSM controller's adaptive uncertainty estimation signal.

Because $\boldsymbol{O}$ is positive definite if $|\boldsymbol{O}| \geq 0, h_{\Psi 1}(c_{\Psi 1}+k_{\Psi 1})-\frac{1}{4} \geq 0$ must be satisfied to ensure that $\dot{V_{\Psi 3}}$ is negative definite when taking the values of $h_{\Psi 1}, c_{\Psi 1}, k_{\Psi 1}$.

$V_{\Psi 3}$ is positive definite and $\dot{V_{\Psi 3}}$ is negative definite, and the system satisfies the conditions of Lyapunov's second method, so it is stable [39].

The stability judgment method of other controllers is similar to this one, as long as the same conditions are satisfied when taking the values of h, h, k the systems will be stable.

IV. SIMULATION RESULT AND ANALYSIS

This section verifies the effectiveness and superiority of the proposed controllers. The effectiveness of a control system is often the most objective criterion for evaluating a controller. To verify the effectiveness of the proposed controller, the proposed adaptive backstepping sliding mode controller was applied to a simulated fixed-wing UAV and compared with the traditional PID control and backstepping slide mode control. By comparing the results of the adaptive backstepping sliding mode control and traditional PID control, a better control performance of the former is achieved. Furthermore, the necessity of adaptive law is reflected in the comparison between the adaptive backstepping sliding mode control and backstepping sliding mode control. The performance comparisons in this section are mainly based on the tracking process of the control signals, control input signals, and adaptive signals.

TABLE 2. Control performance indexes of different yaw angle controllers.

	PID	BSM	ABSM
Stead error	0.29°	-0.05°	0°
Overshoot	0°	1.18°	0°
React time	1.16s	0.49s	0.18s

All controllers should be combined in the simulation process because of the interaction between multiple state variables. Ailerons and rudders, for example, act on roll and yaw motions, and changes in pitch angle also affect altitude and airspeed. The coupling process is so complex that the step simulation is difficult, which, in turn, lead to a significant amount of time spent on parameter selection and adjustment. However, to compare the control effect more clearly, the simulation process was divided into three parts: attitude control, airspeed control, and altitude holding. In each part, the simulation results were compared with the traditional PID control method and the backstepping sliding mode control method.

A. ATTITUDE CONTROLLER SIMULATION

This part presents the control simulation results for the three attitude angles of the fixed-wing UAV. In the simulation of attitude angle control, it is assumed that the initial state airspeed and altitude of the UAV are 60m/s and 2500m, respectively. The effects of attitude control procedures on altitude and airspeed are not discussed in this part. The initial state of the attitude angle (Ψ, θ, Φ) is (0°, 0°, 0°), and the target status is (10°, 10°, 10°).

The parameters of the controller laws in (65), (67), and (69), and the adaptive laws in (66), (68), and (70) are selected as follows:

$$\begin{aligned} &k_{\Psi 1}=60, \quad c_{\Psi 1}=50, \quad h_{\Psi 1}=65, \quad \varepsilon_{\Psi}=1.1, \\ &k_{\Phi 1}=45, \quad c_{\Phi 1}=38, \quad h_{\Phi 1}=55, \quad \varepsilon_{\Phi}=1.2, \\ &k_{\theta 1}=45, \quad c_{\theta 1}=40, \quad h_{\theta 1}=50, \quad \varepsilon_{\theta}=1.5, \\ &\delta_{\Psi}=10, \quad \delta_{\Phi}=28, \quad \delta_{\theta}=30. \end{aligned}$$

For Backstepping Slide Mode control laws:

$$\begin{aligned} &k_{\Psi BSM}=60, \quad c_{\Psi BSM}=50, \quad h_{\Psi BSM}=65, \\ &\varepsilon_{\Psi BSM}=1.1, \quad k_{\Phi BSM}=45, \quad c_{\Phi BSM}=38, \\ &h_{\Phi BSM}=55, \quad \varepsilon_{\Phi BSM}=1.2, \quad k_{\theta BSM}=45, \\ &c_{\theta BSM}=40, \quad h_{\theta BSM}=50, \quad \varepsilon_{\theta \mathrm{BSM}}=1.5, \end{aligned}$$

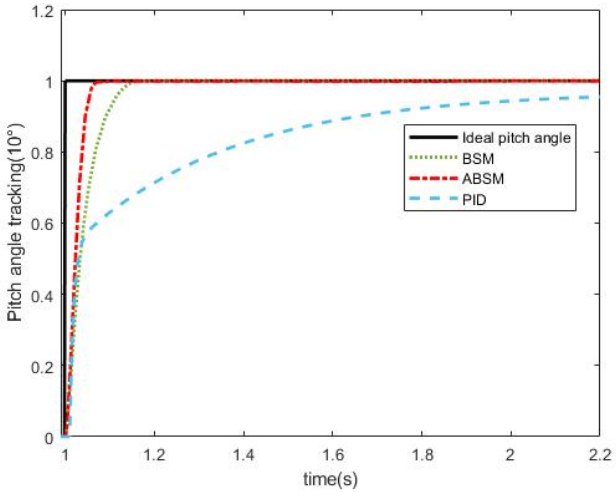

FIGURE 11. Pitch angle tracking comparison.

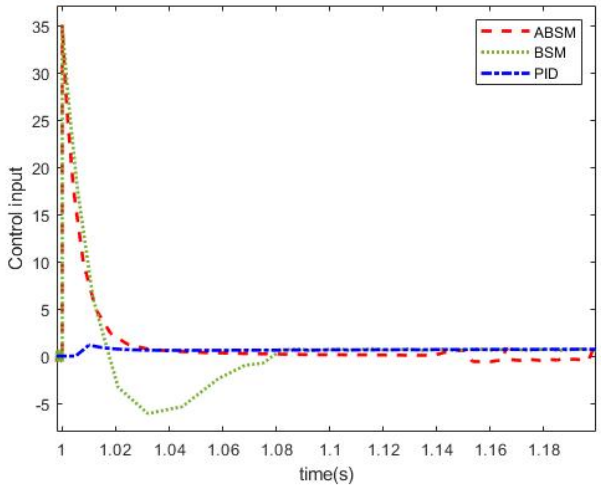

FIGURE 12. Pitch angle controllers' input signal comparison.

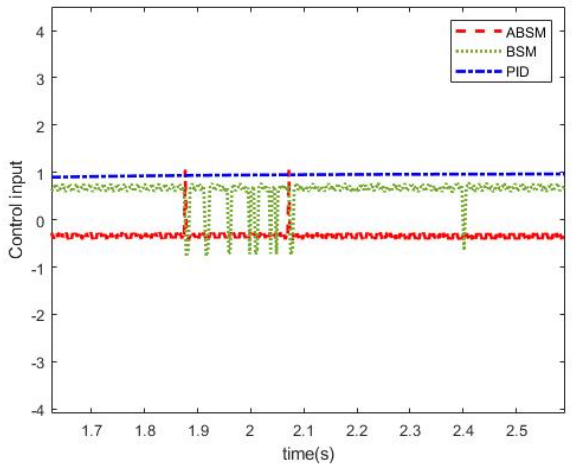

FIGURE 13. Part of Pitch angle controllers' input signal comparison.

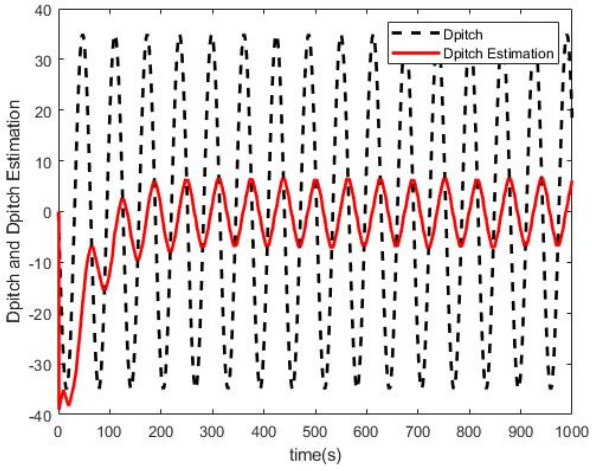

FIGURE 14. Pitch angle ABSM controller's adaptive uncertainty estimation signal.

And for PID control laws:

$$k_{P\Psi} = 8, \quad k_{I\Psi} = 1.7, \quad k_{D\Psi} = 0.5,$$
$$k_{\mathrm{P}\Phi} = 6, \quad k_{\mathrm{I}\Phi} = 1.4, \quad k_{\mathrm{D}\Phi} = 0.2,$$
$$k_{\mathrm{P}\theta} = 5, \quad k_{\mathrm{I}\theta} = 1.8, \quad k_{\mathrm{D}\theta} = 0.4.$$

To achieve a more realistic reaction control effect, the uncertainty data of the system must be obtained from the wind tunnel experiment. According to the wind tunnel test results of the UAV in [28], the total uncertain is taken as

$$D_\Psi = -40sin(0.1t),$$
$$D_\Phi = -30sin(0.1t),$$
$$D_\theta = -35sin(0.1t).$$

The comparison results of the attitude angle simulation control are shown in Figs.4-12. There are three control performance indexes recorded in Table 1-3 to help analyse.

These indexes are stead error, overshoot and react time. From these figures and tables, it is obvious that all three control laws can achieve a stable state for the attitude control of fixed-wing UAVs. However, different control laws exhibit different performances for different attitude angle control processes. Next, the performances of these control laws were analyzed according to different attitude angles.

For the control process of the roll angle, according to Fig.4 and Table 1, the PID control law generates a steady-state error of approximately 0.39° and takes a longer time to reach the steady state. Comparatively, ABSM and BSM reach steady state faster without any steady-state error. Although the reaction speed of BSM is faster, the BSM control law causes an overshoot of approximately 0.32°, which is not allowed for precise control.

A comparison of the input signals of the three control laws is shown in Fig.6. The input signal of the ABSM can reach the steady state smoothly, whereas that of the BSM produces a negative-6.5-overshoot before reaching a steady state. When a large overshoot occurs at the control input signal, it may directly damage the equipment. Therefore, such a situation should be avoided as much as possible during the control

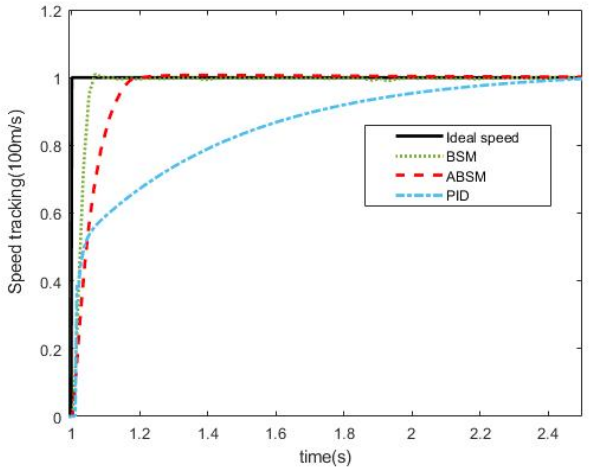

FIGURE 15. Airspeed tracking comparison.

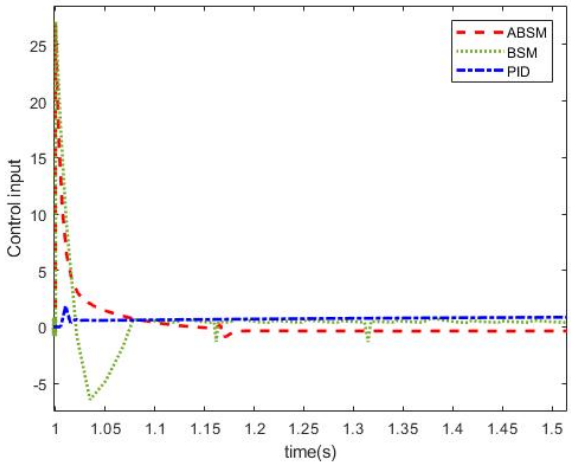

FIGURE 16. Airspeed controllers' input signal comparison.

process. In the roll control process, the ABSM controller has better control performance than the BSM and PID controllers.

For the yaw controller, the situation was similar to that of the roll angle simulation. A more obvious oscillation occurred at the beginning of the BSM tracking signal (shown in Fig.7 and Table 2). The PID control law performs poorly as it does in the roll angle control simulation.

The control input signal was roughly similar to the roll-angle case (Fig.8). It is worth noting that the control input signal of the BSM occurs buffeting after 1.5s (Fig.9). Buffeting is a common phenomenon in sliding mode control and can significantly affect the performance of the controller. The introduction of an adaptive law can not only estimate the uncertainty but also reduce the chattering of the system. Based on the absence of chattering generated by the ABSM in Fig.8, it can be inferred that the design of the chattering reduction system introduced by the adaptive law is effective. Therefore, the performance superiority of the ABSM is reflected.

For the control process of the pitch angle, PID steady-state error still exists, and the control speed and accuracy

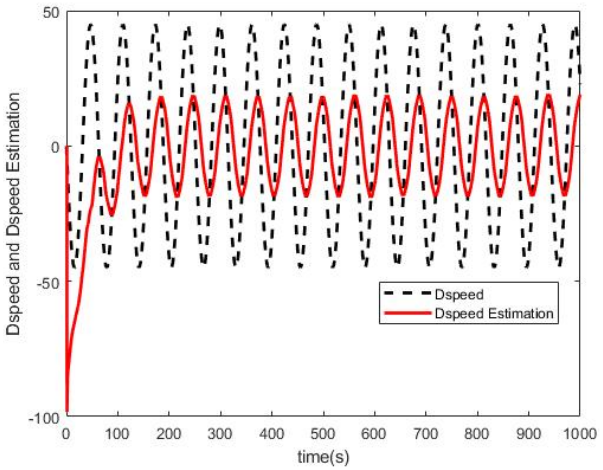

FIGURE 17. Airspeed ABSM controller's adaptive uncertainty estimation signal.

TABLE 3. Control performance indexes of different pitch angle controllers.

	PID	BSM	ABSM
Stead error	-0.41°	-0.01°	0°
Overshoot	0°	0.02°	0°
React time	1.19s	0.17s	0.14s

of ABSM and BSM are close (Fig.11 and Table 3). However, it is worth noting that the known upper limit of the disturbance is a necessary condition when designing a BSM controller, while an ABSM controller can be obtained without this condition. In practice, the upper limit of the disturbance is often unpredictable; therefore, ABSM is still the better choice.

The input signal is similar to that of the previous two control processes. Although slight chattering also occurs in the ABSM between 1.9s and 2.1s, the effect of using the adaptive law to reduce chattering is significant when compared with the BSM input signal (Fig.12 and 13).

The signals of the adaptive law are shown in Fig.6, 10, and 14. It can be observed that the adaptive signals will try to follow the disturbance when the system inputs the step signal, and then it can follow the sinusoidal uncertain signal periodically after entering the steady state.

B. AIRSPEED CONTROL SIMULATION

This part presents the simulation results of the airspeed control. During the airspeed simulation, to reduce the influence of system disturbance on airspeed control, the attitude angles were fixed. Both the roll and yaw angles were set to 0 rad, and the pitch angle was fixed at 10 rad. The initial value of the airspeed was 0 m/s, and the target value was 100 m/s. The effect of airspeed control on altitude was not the focus of this part of study.

The total uncertainty of the airspeed control system must be selected prior to the simulation. The method of uncertainty cited was the same as that used in Section IV.A, where the

TABLE 4. Control performance indexes of different airspeed controllers.

	PID	BSM	ABSM
Stead error	0.02°	-0.03°	0.03°
Overshoot	0°	1.11°	0°
React time	1.18s	0.14s	0.27s

uncertainty is selected as

$$D_v = -45sin(0.1t)$$

Other parameters related to the airspeed controllers are selected as follow:

For Adaptive Backstepping Slide Mode

$$k_{A1} = 40, \quad c_{A1} = 30, \quad h_{A1} = 45, \quad \varepsilon_A = 1.5, \quad \delta_A = 35.$$

For Backstepping Slide Mode control laws:

$$k_{ABSM} = 40, \quad c_{ABSM} = 30, \quad h_{ABSM} = 45, \quad \varepsilon_{ABSM} = 1.5.$$

And for PID control laws:

$$k_{PA} = 4, \quad k_{IA} = 0.6, \quad k_{DA} = 0.1.$$

A performance comparison of the three controllers in the airspeed control process is shown in Fig.15 and Table 4. The tracking speed of ABSM and BSM is still faster than that of PID, and there is no steady-state error after reaching a steady state. Comparing the ABSM with the BSM control, the BSM has a faster response time as well as a small overshoot. According to the stability principle, the ABSM exhibits better performance and does not need to determine the upper limit of the disturbance in advance.

Even though the airspeed-following performance of the BSM controller can be regarded as good, the input signal has buffeting, as shown in Fig.16, which poses a risk to the stability of the system. However, there is no chattering in the input signal of the ABSM, and its adaptive signal periodically follows the uncertainty of the system after the system reaches a steady state (Fig.17). Therefore, in the process of airspeed control, ABSM is still the controller with the best control performance.

C. ALTITUDE HOLDING CONTROL SIMULATION

This section mainly analyzes the simulation results of the coupled height controller. It mainly simulates the process of controlling the height with the pitch angle in the height-holding area.

The airspeed was kept constant at 60 m/s, and the roll angle and yaw angle were set to 0°. The initial height was 2500m, and the coupling controller controlled the altitude of the UAV to 2600m. The airspeed was kept constant; therefore, there was no additional perturbation to the altitude. Because the height-keeping controller is a coupling controller, the control performance of different control laws is slightly different from that of the previous control laws.

The parameters of the primary PID controller are selected as follows:

$$k_v = 15, \quad k_v = 3.5, \quad k_v = 1.6.$$

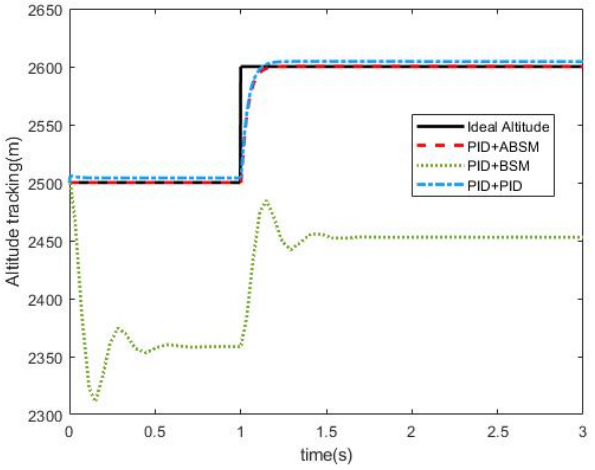

FIGURE 18. Altitude tracking comparison of coupled controllers.

TABLE 5. Control performance indexes of different altitude coupled controllers.

	PID	BSM	ABSM
Stead error	4.17m	-47.19m	0.43m
Overshoot	0m	31.77m	0m
React time	0.23s	0.19s	0.62s

The second controller adopted the pitch angle controllers designed in the previous attitude control simulation.

The initial value was 2500m. After the steady state was reached, the command signal was changed to 2600m. As shown in Fig.18 and Table 5, the coupling controller of the BSM produces an irredeemable steady-state error (−47.19m) and a small shock caused by the buffeting. Compared with PID-BSM, the control effects of the lower cascade PID controller and the PID-ABSM coupling controller are better.

Both the PID-PID controller and PID-ABSM controller have good control performance, although the former has a state error within ±5m. However, the PID-PID control needs to know the precise parameters and disturbances of the controlled system, and the PID-ABSM coupling controller can overcome this limitation with an adaptive law. Therefore, the performance of the PID-ABSM coupling controller still performs better than the other two controllers in the height-keeping control process.

V. CONCLUSION

In this study, a fixed-wing-UAV controller that combines adaptive method and backstepping sliding mode was designed and simulated. Compared with previous sliding mode controllers, this controller can overcome the uncertainty of system parameters as well as the external disturbances and eliminate chattering at the same time by an adaptive law. The fixed-wing UAV model is a nonlinear, multi-state coupling and extremely complex model. Furthermore, owing to the influence of various disturbances and uncertainties, it is difficult to control a fixed-wing UAV well. Therefore, it is recommended to use this design for

an improvement on control performance. Its stability has been proved using Lyapunov's second method. Moreover, how to select relevant parameters to ensure stability has been specified.

The simulation results verified the effectiveness and stability of the controllers. The advantages of ABSM control method are demonstrated in comparison with the PID and BSM control methods. Although the system is multi-variable and multi-coupled, it is feasible to design the controller separately for a single variable by decoupling analysis. The adaptive system is used to suppress the buffeting and estimate the uncertainty of the system and external disturbances. The effectiveness and traceability of the adaptive laws were verified using simulation results.

In future work, we plan to apply the designed controller to a real fixed-wing UAV. The principle is to input the control algorithm into the STM32 chip and design the related hardware system. Planning ground station software to complete specific flight missions.

REFERENCES

[1] S. R. B. dos Santos, C. L. N. Júnior, S. N. G. Junior, A. Bittar, and N. M. F. de Oliveira, "Experimental framework for evaluation of guidance and control algorithms for UAVs," in *Proc. 21st Brazilian Congr. Mech. Eng.*, Natal, Brazil, 2011, pp. 1–10.

[2] K. T. Öner, "Mathematical modeling and vertical flight control of a tilt-wing UAV," *Turkish J. Elect. Eng. Comput. Sci.*, vol. 20, no. 1, pp. 149–157, 2012.

[3] T. S. No, B. M. Min, R. H. Stone, and K. C. Wong, "Control and simulation of arbitrary flight trajectory-tracking," *Control Eng. Pract.*, vol. 13, no. 5, pp. 601–612, May 2005.

[4] S. Islam, P. X. Liu, and A. El Saddik, "Nonlinear adaptive control for quadrotor flying vehicle," *Nonlinear Dyn.*, vol. 78, no. 1, pp. 117–133, 2014.

[5] S.-T. Zhao and X.-W. Gao, "Robust adaptive control for a class of uncertain non-affine nonlinear systems using neural state feedback compensation," *J. Central South Univ.*, vol. 23, no. 3, pp. 636–643, Mar. 2016.

[6] X. Bu, X. Wu, Z. Ma, and R. Zhang, "Nonsingular direct neural control of air-breathing hypersonic vehicle via back-stepping," *Neurocomputing*, vol. 153, pp. 164–173, Apr. 2015.

[7] F. Rinaldi, S. Chiesa, and F. Quagliotti, "Linear quadratic control for quadrotors UAVs dynamics and formation flight," *J. Intell. Robotic Syst.*, vol. 70, nos. 1–4, pp. 203–220, 2013.

[8] Y. Kang and J. K. Hedrick, "Linear tracking for a fixed-wing UAV using nonlinear model predictive control," *IEEE Trans. Control Syst. Technol.*, vol. 17, no. 5, pp. 1202–1210, Apr. 2009.

[9] L. Wang, Y. He, Z. Zhang, and C. He, "Trajectory tracking of quadrotor aerial robot using improved dynamic inversion method," *Intell. Control Autom.*, vol. 4, no. 4, pp. 343–348, 2013.

[10] P. C. Garcia, P. Castillo, R. Lozano, and A. E. Dzul, *Modelling and Control of Mini-Flying Machines*. London, U.K.: Springer, 2005.

[11] M. M. Nicotra, E. Garone, R. Naldi, and L. Marconi, "Nested saturation control of an UAV carrying a suspended load," in *Proc. Amer. Control Conf.*, Jun. 2014, pp. 3585–3590.

[12] A. Mokhtari, N. K. M'Sirdi, K. Meghriche, and A. Belaidi, "Feedback linearization and linear observer for a quadrotor unmanned aerial vehicle," *Adv. Robot.*, vol. 20, no. 1, pp. 71–91, Jan. 2006.

[13] I. Choi and H. Bang, "Quadrotor-tracking controller design using adaptive dynamic feedback-linearization method," *Proc. Inst. Mech. Eng., G, J. Aerosp. Eng.*, vol. 228, no. 12, pp. 2329–2342, Oct. 2014.

[14] T. Madani and A. Benallegue, "Control of a quadrotor mini-helicopter via full state backstepping technique," in *Proc. 45th IEEE Conf. Decis. Control*, Dec. 2006, pp. 1515–1520.

[15] C. S. Ha, Z. Zuo, F. B. Choi, and D. Lee, "Passivity-based adaptive backstepping control of quadrotor-type UAVs," *Robot. Auton. Syst.*, vol. 62, no. 9, pp. 1305–1315, Sep. 2014.

[16] M. Ö. Efe, "Battery power loss compensated fractional order sliding mode control of a quadrotor UAV," *Asian J. Control*, vol. 14, no. 2, pp. 413–425, 2012.

[17] R. Xu and Ü. Özgüner, "Sliding mode control of a class of underactuated systems," *Automatica*, vol. 44, no. 1, pp. 233–241, Jan. 2008.

[18] C. Zhang, G. Zhang, and Q. Dong, "Multi-variable finite-time observer-based adaptive-gain sliding mode control for fixed-wing UAV," *IET Control Theory Appl.*, vol. 15, no. 2, pp. 223–247, Jan. 2021.

[19] T. Espinoza, A. E. Dzul, R. Lozano, and P. Parada, "Backstepping-sliding mode controllers applied to a fixed-wing UAV," *J. Intell. Robot. Syst.*, vol. 73, no. 1, pp. 67–79, 2014.

[20] C. Herman, O. S. Salas-Peña, and L. de León-Morales, "Extended observer based on adaptive second order sliding mode control for a fixed wing UAV," *ISA Trans.*, vol. 66, pp. 226–232, Jan. 2017.

[21] L. Melkou, M. Hamerlain, and A. Rezoug, "Fixed-wing UAV attitude and altitude control via adaptive second-order sliding mode," *Arabian J. Sci. Eng.*, vol. 43, no. 12, pp. 6837–6848, Dec. 2018.

[22] X. Qiu, M. Zhang, W. Jing, and C. Gao, "Dynamics and adaptive sliding mode control of a mass-actuated fixed-wing UAV," *Int. J. Aeronaut. Space Sci.*, vol. 22, no. 4, pp. 886–897, Aug. 2021.

[23] K. Wu, Z. Cai, J. Zhao, and Y. Wang, "Target tracking based on a nonsingular fast terminal sliding mode guidance law by fixed-wing UAV," *Appl. Sci.*, vol. 7, no. 4, p. 333, Mar. 2017.

[24] X. Wang, Y. Yu, and Z. Li, "Distributed sliding mode control for leader-follower formation flight of fixed-wing unmanned aerial vehicles subject to velocity constraints," *Int. J. Robust Nonlinear Control*, vol. 31, no. 6, pp. 2110–2125, Apr. 2021.

[25] Y. Han, P. Li, and Z. Zheng, "A non-decoupled backstepping control for fixed-wing UAVs with multivariable fixed-time sliding mode disturbance observer," *Trans. Inst. Meas. Control*, vol. 41, no. 4, pp. 963–974, Feb. 2019.

[26] Z. Zheng, Z. Jin, L. Sun, and M. Zhu, "Adaptive sliding mode relative motion control for autonomous carrier landing of fixed-wing unmanned aerial vehicles," *IEEE Access*, vol. 5, pp. 5556–5565, 2017.

[27] X. Jiang, C. Su, Y. Xu, K. Liu, H. Shi, and P. Li, "An adaptive backstepping sliding mode method for flight attitude of quadrotor UAVs," *J. Central South Univ.*, vol. 25, no. 3, pp. 616–631, 2018.

[28] R. W. Beard and T. W. McLain, *Small Unmanned Aircraft*. Princeton, NJ, USA: Princeton Univ. Press, 2012.

[29] S. V. Shkarayev, P. G. Ifju, J. C. Kellogg, and T. J. Mueller, *Introduction to the Design of Fixed-Wing Micro Air Vehicles Including Three Case Studies*. New York, NY, USA: AIAA, 2007.

[30] T. J. Mueller, *Fixed and Flapping Wing Aerodynamics for Micro Air Vehicle Applications*. Reston, VA, USA: AIAA, 2001.

[31] A. Brezoescu, R. Lozano, and P. Castillo, "Lyapunov-based trajectory tracking controller for a fixed-wing unmanned aerial vehicle in the presence of wind," *Int. J. Adapt. Control Signal Process.*, vol. 29, no. 3, pp. 372–384, 2015.

[32] X.-X. Hu, Y. Chen, and H. Luo, "Robust decision making for UAV air-to-ground attack under severe uncertainty," *J. Central South Univ.*, vol. 22, no. 11, pp. 4263–4273, Nov. 2015.

[33] T. Z. Muslimov and R. A. Munasypov, "Consensus-based cooperative control of parallel fixed-wing UAV formations via adaptive backstepping," *Aerosp. Sci. Technol.*, vol. 109, Feb. 2021, Art. no. 106416.

[34] P. R. Ambati and R. Padhi, "Robust auto-landing of fixed-wing UAVs using neuro-adaptive design," *Control Eng. Pract.*, vol. 60, pp. 218–232, Mar. 2017.

[35] L. Long and J. Zhao, "H_∞ control of switched nonlinear systems in p-normal form using multiple Lyapunov functions," *IEEE Trans. Autom. Control*, vol. 57, no. 5, pp. 1285–1291, May 2012.

[36] M. A. Duarte-Mermoud, N. Aguila-Camacho, J. A. Gallegos, and R. Castro-Linares, "Using general quadratic Lyapunov functions to prove Lyapunov uniform stability for fractional order systems," *Commun. Nonlinear Sci. Numer. Simul.*, vol. 22, pp. 650–659, May 2015.

[37] B.-Z. Guo and J.-J. Liu, "Sliding mode control and active disturbance rejection control to the stabilization of one-dimensional Schrödinger equation subject to boundary control matched disturbance," *Int. J. Robust Nonlinear Control*, vol. 24, no. 16, pp. 2194–2212, Nov. 2014.

[38] A. A. Martynyuk and Y. A. Martynyuk-Chernienko, *Uncertain Dynamical Systems: Stability and Motion Control*, 1st ed. Boca Raton, FL, USA: CRC Press, 2011.

[39] A. A. Martyniuk, *Stability of Motion: The Role of Multicomponent Liapunov's Functions*. Cambridge, U.K.: CSP, 2007.

CHANGCHUN BAO was born in Inner Mongolia, China, in 1980. He received the B.S. degree in materials science and engineering and the M.S. degree in engineering mechanics from the Inner Mongolia University of Technology, Hohhot, China, in 2004 and 2009, respectively, and the Ph.D. degree in aeronautical and astronautical engineering from Tsinghua University, Beijing, China, in 2019.

From 2010 to 2019, he was a Research Assistant with the Engineering Mechanics Laboratory, Inner Mongolia University of Technology. Since 2019, he has been an Assistant Professor with the Aviation Engineering Department, Inner Mongolia University of Technology. He also co-founded and served as the Deputy General Manager for Beijing Qinghang Bauhinia Equipment Technology Company Ltd. He has authored five articles and more than ten inventions. His research interests include spacecraft dynamics and control, aircraft design, control system design, complex aircraft modeling, aircraft dynamics analysis, and spacecraft control system design.

Dr. Bao won the overall Champion Award of the 5th China ''Internet +'' College Students Innovation and Entrepreneurship Competition, in October 2019, and was selected into the Inner Mongolia New Century 321 Talent Project.

YUFEI GUO was born in Hohhot, Inner Mongolia, China, in 1996. He received the bachelor's degree in automation from the Inner Mongolia University of Technology, Hohhot, China, in 2014, and the master's degree in electrical engineering from the University of New South Wales (UNSW), Sydney, Australia, in 2020.

From 2014 to 2018, he was a Research Assistant with the Automation Laboratory, Inner Mongolia University of Technology. Since 2019, he has been an Assistant with the Electrical Engineering Laboratory, UNSW. His research interests include nonlinear systems, flight vehicle design, automatic control system design, design of sliding mode controller, and system stability analysis.

Mr. Guo's awards include the Second Prize of the 14th China College Student Robot Competition, the China Robot Competition and ''Robo Cup''-Open Medical and Service Robot Orthopedic Surgery Project, and the Third Prize of the 14th National College Student Robot Competition ROBOMASTERS North China Division.

LERU LUO received the B.S. degree in aircraft design and engineering from the Harbin Institute of Technology, Harbin, China, in 2020. She is currently pursuing the M.S. degree in dynamics and control with the Inner Mongolia University of Technology, Inner Mongolia, China.

Her research interests include spacecraft attitude control, helicopter control, UAV attitude control, and modern control theories.

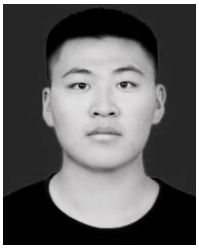

GUANQUN SU was born in Chifeng, Inner Mongolia Autonomous Region, China, in 1997. He received the B.Sc. degree from the School of Mathematical Science, Heilongjiang University, in 2019. He is currently pursuing the master's degree in engineering from the College of Electronic and Information Engineering, Inner Mongolia University.

From 2015 to 2019, he was a Research Assistant with the Computational Mathematics Laboratory, Heilongjiang University. His research interests include stability of control systems, consistency of multi-agent systems, and time-delay systems.

Mr. Su's awards and honors include the Outstanding Graduate of Heilongjiang University and the Academic Scholarship of Inner Mongolia University.